Received 13 October 2018; | Revised 13 October 2018; | Accepted 13 October 2018

DOI: xxx/xxxx

STRUCTURAL CONTROL AND HEALTH MONITORING

Evaluation of optimal analysis, design and testing of electromagnetic shunt damper for vibration control of a civil structure†

Wai Kei Ao*[1] | Paul Reynolds[2]

[1]Vibration Engineering Section, College of Engineering, Mathematics and Physical Sciences, University of Exeter, Exeter, United Kingdom

[2]Vibration Engineering Section, College of Engineering, Mathematics and Physical Sciences, University of Exeter, Exeter, United Kingdom

Correspondence
*Wai Kei Ao Email: wka203@exeter.ac.uk

Present Address
North Park Road, Exeter EX4 4QF, UK.

Summary

The current study is to find out alternative damping to provide satisfactory vibration suppression performance in civil engineering. Accordingly, electromagnetic actuators and electromagnetic dampers (EMDs) are utilised to generate electromagnetic damping. For further discussion on control of vibration serviceability problem in civil structure, the use of a linear voice coil motor (LVCM) as an EMD is implemented to attenuate unwanted vibration.

To induce appropriate electromagnetic damping the terminal ends of the LVCM need to connect with shunt circuits. The basic resistor series circuit and resistor, inductor and capacitor (RLC) oscillating circuit are employed to connect to the LVCM in term of enhancing the EMD damping. However, a design of the electromagnetic shunt damper (EMSD) is required with the generic H_∞ and H_2 robust optimisation techniques to determine shunt circuit components, in which the results of these optimisations were discussed on the previous author study.

For extending the EMSD study, the resulting EMSD is experimentally exploited to a six-storey aluminium frame structure. The random and harmonic excitations are selected to input to the structure to examine the performance of the electromagnetic damping. The finding of the experimental test of the EMSD gives satisfactory vibration suppression performance.

KEYWORDS:
Tuned mass damper (TMD), Electromagnetic damper (EMD), Electromagnetic shunt damper (EMSD), RLC resonant circuit, H_∞ optimisation, H_2 optimisation, Nonlinearity

1 | INTRODUCTION

Use of electromagnetic dampers (EMDs) to generate electromagnetic force or damping is based on electromagnetic induction theory. EMDs can be used for vibration suppression and are widely utilised in mechanical systems and railway braking systems. Eddy current damping has also been successfully used in suppressing unwanted vibration. However, in civil engineering structures, it has been common to use more traditional dampers such as viscous dampers (VDs) and tuned mass dampers (TMDs).

†Evaluation of optimal analysis, design and testing of electromagnetic shunt damper for vibration control of a civil structure.

[0]**Abbreviations:** EMD, electromagnetic damper; EMSD, electromagnetic shunt damper; LVCM, linear voice coil motor; VD, viscous damper; TMD, tuned mass damper; AMRF, aluminium moment resisting frame

A VD provides additional passive damping to a structure and hence reduces the amplitude of the dynamic response. Also, a TMD can be used for passive vibration control by adding an additional SDOF system (mass, stiffness, damping) to the primary structure. A TMD is designed to split a high magnitude resonant peak in the system FRF down to two lower peaks. A larger mass ratio can achieve better vibration mitigation, but in practice a mass ratio greater than 5 % is hard to achieve. In this study, an EMD is selected as an alternative to a TMD to overcome these challenges.

The fundamental electromagnetic damping concept of EMDs was proposed by [7, 6] and electromagnetic damping was presented in a passive manner to provide equivalent damping. A shunt impedance circuit was used in series with the EMD, to provide good electromagnetic shunt damping to the mass spring damper system. After this simple passive control, [19, 20] proposed and created an electromagnetic transducer for performing passive and advanced active robust control. The electromagnetic transducer acts as an EMD, constructed using two electromagnetic coils, to reduce the vibration problem in the host structure.

A flexible aluminium cantilever beam was studied by [11]. An electromagnetic shunt damper (EMSD) was passively suspended from the end of the beam to reduce vibration, and an RC resonant shunt circuit was connected in series with the EMD. An experiment by [26] used a capacitor inductor circuit and a negative resistor capacitor inductor circuit to attenuate the disturbance of the cantilever beam. Another study by [25, 10] used an RLC resonant shunt circuit to achieve vibration suppression of the flexible cantilever beam. Otherwise, for creating broadband damping, [36, 35] proposed negative impedance shunts and negative inductance negative impedance to improve the damping effect of electromagnetic shunt damping.

An electromagnetic voice coil motor was adopted to connect resistor-capacitor (RC) resonant shunt circuit and performed active control [22, 23]. The proper controller design was implemented by relevant optimal circuit components tuning, which could provide broadband controllable shunt stiffness and damping to mitigate the undesirable disturbance. This type of actively EMSD can achieve as similar as dynamic behaviour of a TMD. The EMSD feature can separate a modal peak into two lower peaks at lower and higher frequencies.

Paper [38] installed a mass-spring-damper on the main structure and implemented a numerical study, while the damping component was provided by EMD with resistor-inductor-capacitor (RLC) shunt circuit. The decentralized H_2 robustness control was utilised to select optimal circuit components and tuned the coupling coefficient of the EMSD. A mathematical model was employed and verified the TMD with EMSD could have series TMD dynamic performance as well as provide passively vibration suppression and energy harvesting objective. Paper [16] used an electromagnetic transducer (piezoelectric transducer) with a resistor-inductor (RI) shunt circuit as an energy harvester and connected to a mass-spring-damper system. The base and force excitation were driving to the system. Once varying the value of shunt impedance, the effect of electromagnetic coupling was varied and achieved different levels of electrical power harvested as well as facilitated vibration attenuation.

An active electromagnetic vibration absorber was developed to achieve energy recovery and frequency tuning objective [21]. The mechanism of the system was chosen electromagnetic transducer and series shunt RLC circuits. The selected capacitor and inductor were given wideband frequency range returning and shifting, which could achieve tuned and harvested the electrical power and reduced maximum displacement of the host structure. Also, a passive vibration absorber with eddy current damping was applied to perform vibration suppression numerically and experimentally [5]. The optimal damping design could increase the system damping and induced the dynamic feature of the absorber as a TMD, which did not require any external energy source to change the absorber device.

A brushless DC machine was adopted as a force actuator to apply in the civil engineering for structural response reduction [29]. The concept was to convert mechanical energy (linear force and velocity external input) to electrical energy (electric motor) via linear rotational conversation system (gear reducer and ball-screw mechanism). The terminal of the motor was collected to active and semiactive circuitry to achieve a controllable damping coefficient. Based on the findings from this study, Scruggs et al. [30, 31] extended the work and proposed regenerative force actuation (RFA) networks, which was groups of electromagnetic force actuators. The RFA was required minimal external power. The idea of the group of actuators was to share power. It means that one device was used to remove vibrating energy at one location of the structure and re-inject some that of energy back into the structure at a different location from other actuators. The excessive removal energy from the vibrating structure was dissipated through the electrical resistor bank. This generalised model of the RFA was numerically applied to a three-storey scale model building under the seismic excitation. It is shown that this type of energy recover actuation networks could improve overall structural dynamic performance.

A numerical study of passive electromagnetic shock absorbers (linear displacement motors) implemented to a building for mitigating the unexpected disturbance [27, 28]. The motor was connected to each level in the horizontal direction, in which the terminal of the motor connected with different impedance shunt circuits. The activated linear displacement motor converted the mechanical energy to electrical energy via electromagnetic coupling effect and then induced electromagnetic force (damping

force), which was the negative direction of the motion. Based on several case studies, the dynamic feature of the passive electromagnetic shock absorber with impedance shunt circuit was the same or beyond a VD when the proper impedance connected. Paper [8] was selected a back-driven ball screw electromagnetic transducer with a permanent magnet synchronous machine for large-scale energy harvesting application of vibrating structures. A TMD device was selected to connect to the transducer when the TMD was vibrating that vibratory energy from the main structure (e.g. multistory buildings and bridges) transformed to TMD, and then the transducer would simultaneously activate and could harvest. The energy harvested from the vibration energy was numerically and experimentally verified, which could potentially use for powering wireless sensing and provide the power for the semi-active control device. Another type of ball screw rotating internal mass electromagnetic damper was developed to provide seismic resistance of a three-storey shaking table test [24]. The ball screw passively converted the axial oscillation of the rod end into rotational motion via an internal flywheel and activated inertial power generator. The terminal of the generator connected to a resistor; therefore, the inertial force and the electromagnetic damping force could be generated semi-actively. Using the forces could successfully control the dynamic response of each level.

In previous studies by [37] and [2, 3], the authors examined an EMD connected in series with an RLC resonant circuit. The dynamic response is analogous with an equivalent TMD. Zhu et al. [37] discussed H_∞ optimisation design, whereas [2, 3] included both H_∞ and H_2 robust optimisation control design methods. This study extends the work of those papers and uses the in findings for application to a laboratory scale structure to evaluate this damper design methodology.

The first section of this paper discusses the motivation behind this study including the merits and demerits of traditional dampers in comparison with electromagnetic dampers. The second section briefly reviews TMD theory including the H_∞ and H_2 robust optimisation designs. The next section discusses the behaviour of an EMD connected with a basic shunt circuit and covers the dynamic characteristics of the EMSD. The fourth section introduces the moment-resisting frame and data acquisition system used for the practical study of an EMSD, including modal testing, EMSD application and performance evaluation. Finally, the last section summarises the results of the EMSD study and gives recommendations for further work.

2 | CONVENTIONAL PASSIVE DAMPING TECHNOLOGIES

2.1 | Viscous dampers (VDs)

The equation of motion of mechanical system can be expressed as mass-spring-damper model. To improve the behaviour of the system, these three components can be used to adjust in terms of achieving a better dynamic performance. One of the solution is to use a passive liquid viscous damper increasing the system damping [33, 9]. A linear liquid viscous damper is shown in Figure 1 a, which is commonly used in civil engineering. The use of this damper can provide a proper damping force without any additional stiffening effect (storage stiffness).

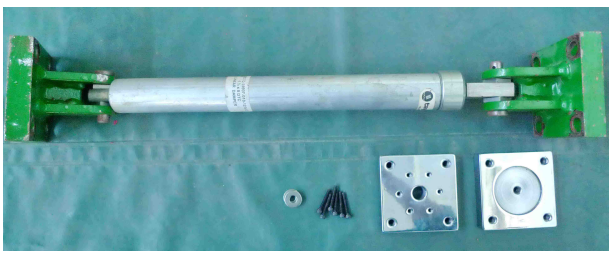

(a) Photo of linear fluid viscous damper

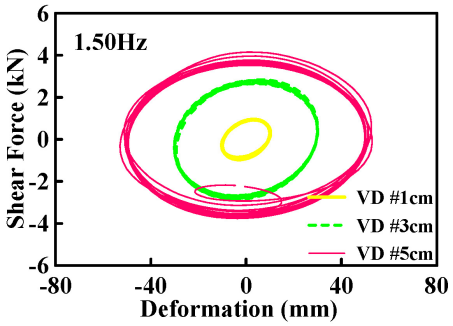

(b) Hysteresis loop of VDs

FIGURE 1 Photo of viscous damper and hysteresis loop demonstration [4]

The damping force of liquid viscous dampers is related to the relative velocity, which is given by:

$$F_D = C|\dot{u}|^{\alpha}\mathrm{sgn}(\dot{u}) \tag{1}$$

where F_D is a damping force of VDs. C is a damping coefficient of VDs. $\dot{u}$ is a relative velocity of piston movement. α is a nonlinear coefficient. sgn($\dot{u}$) is a sign convention depending on the velocity. When $\dot{u} \geq 0$, then sgn($\dot{u}$) $= +1$. Whilst, $\dot{u} < 0$, then sgn($\dot{u}$) $= -1$.

Figure 1 b is a hysteresis loop demonstration picking 1.5 Hz with different displacement control. The shape of the hysteresis loop is closed to ellipse shape, which can be shown that VDs has no storage stiffness.

In the design process, FEMA (Federal Emergency Management Agency) in October 1997 published FEMA273 and 274 of the NEHRP (National Earthquake Hazard Reduction Program) specification [18, 17]. They were written to discuss and specify passive devices for reduction of structural response. The effective damping ratio estimation formula was also proposed from FEMA 273, which is given by:

$$\zeta_{eff} = \zeta_0 + \zeta_d = \zeta_0 + \frac{T \sum_j C_j \cos^2\theta_j {\varphi_{rj}}^2}{4\pi \sum_i m_i {\varphi_i}^2} \tag{2}$$

where T is the first mode period of the system, m_i is the mass of the i^{th} degree of freedom, ϕ_i is the displacement of the i_{th} degree of freedom of the first vibration mode, ϕ_{rj} is horizontal relative displacement of the j^{th} device at the first vibration mode and θ_j is the horizontal inclined angle of the j^{th} installed damper device.

2.2 | Tuned mass dampers (TMDs)

Over the last two decades, tuned mass dampers have been used in many studies and applications in civil engineering. The benefit of using TMDs is consisting of a simple components: mass source, stiffness and dashpot. Using these three main components alongside proper design methods, the TMDs can deal with plenty of unexpected disturbance. The mechanics of TMDs can represent a two degrees of freedom system in horizontal direction as seen in Figure 2 .

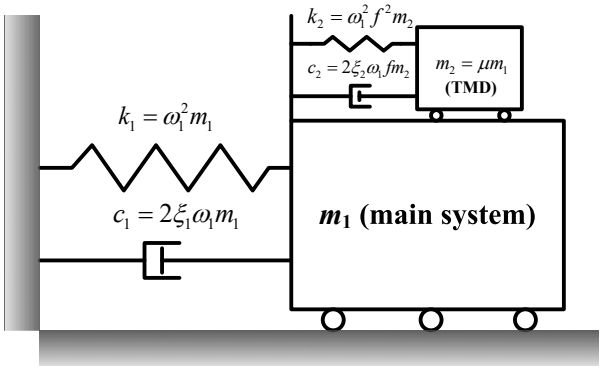

FIGURE 2 Tuned mass damper demostration in horizontal direction [4]

The main system in Figure 2 represents the original structure, like a moment resisting frame (MRF). The additional mass m_2, stiffness k_2 and damping coefficient c_2 are the main consisting components of TMDs. The relevant equation of motion of single degree of freedom TMDs can be written as follows [15]:

$$\begin{bmatrix} m_1 & 0 \\ 0 & m_2 \end{bmatrix} \begin{Bmatrix} \ddot{x}_1 \\ \ddot{x}_2 \end{Bmatrix} + \begin{bmatrix} c_1 + c_2 & -c_2 \\ -c_2 & c_2 \end{bmatrix} \begin{Bmatrix} \dot{x}_1 \\ \dot{x}_2 \end{Bmatrix} + \begin{bmatrix} k_1 + k_2 & -k_2 \\ -k_2 & k_2 \end{bmatrix} \begin{Bmatrix} x_1 \\ x_2 \end{Bmatrix} = \begin{Bmatrix} f \\ 0 \end{Bmatrix} \tag{3}$$

To acquire optimal control, two fundamental robust optimisation methods H_∞ and H_2 are selected. Those methods are commonly used in the design of optimal parameters. Before performing the optimal process, the time domain state space needs to be transformed to the Laplace domain state space, which is convenient for obtaining the frequency response information of the TMD system between output and input, respectively. It can be expressed as

$$\frac{X_1(s)}{F(s)} = \frac{s^2 + 2\xi_2\omega_2 s + {\omega_2}^2}{m_1 s^4 + \left(2\xi_2 m_2\omega_2 + c_1 + c_2\right) s^2 + \left(m_1{\omega_2}^2 + 2\xi_2\omega_2 c_1 + k_1 + k_2\right) s^2 + \left(c_1{\omega_2}^2 + 2\xi_2\omega_2 k_1\right) s + {\omega_2}^2 k_1} \tag{4}$$

For further applications, equation 4 can be rewritten as mass ratio , $\mu = \frac{m_2}{m_1}$ and two frequency ratios , $\gamma = \frac{\omega_2}{\omega_1}$ and $\lambda = \frac{\omega}{\omega_1}$ [15]. It is shown as follows:

$$H(\lambda) = \frac{X_1(\lambda)}{F(\lambda)/k_1} = \frac{\gamma^2 - \lambda^2 + j2\xi_2\gamma\lambda}{\lambda^4 + \gamma^2 - \gamma^2\lambda^2 - \lambda^2 - \mu\gamma^2\lambda^2 + j\left(-2\xi_2\gamma\lambda^3 - 2\xi_2\mu\gamma\lambda^3 + 2\xi_2\gamma\lambda\right)} \tag{5}$$

Den Hartog [15] and [34] derived the H_∞ optimisation design to the frequency response function (FRF) peak of significant frequency range. The optimal frequency ratio and damping ratio can be expressed as

$$\gamma_{opt} = \frac{1}{1+\mu} \tag{6}$$

$$\xi_{2,opt} = \sqrt{\frac{3\mu}{8(1+\mu)}} \tag{7}$$

On the other hand, [12] proposed the H_2 robust optimisation method to find the average total energy in a wide frequency bandwidth. The relative optimal frequency and damping ratio can be written as

$$\gamma_{opt} = \sqrt{\frac{\mu+2}{2(\mu+1)^2}} \tag{8}$$

$$\xi_{opt} = \frac{1}{2}\sqrt{\frac{\mu(3\mu+4)}{2(\mu+2)(\mu+1)}} \tag{9}$$

It is noted that the H_∞ and H_2 optimal frequency and damping ratios have different equation expressions but all of them are a function of the mass ratio (TMD mass to main system mass). From this point of view, choosing a different mass ratio can induce a different vibration absorption.

3 | ELECTROMAGNETIC DAMPER WITH SHUNT CIRCUIT (EMSD)

The first part of this section introduces the mechanism of the mechanical system with an EMSD using an impedance shunt circuit. The second part of this section explains an alternative type of shunt circuit; an RLC resonant shunt circuit.

Figure 3 a shows a conceptual diagram of an EMD, which essentially is a linear voice coil motor (LVCM). The ring magnets of the EMD are mounted inside the tube shell, which can be metal or nonmetal material. The conductive coil forms the core of the EMD. A small gap exists between the magnetic tube shell and the coil, which allows the coil moving in the axial direction to cut through magnetic lines within the stroke of the LVCM. Electromagnetic induction will generate an induced electromotive force (emf). A typical voltage time history (induced emf) is shown in Figure 3 b. The AC voltage shown corresponds with reciprocal motion of the coil.

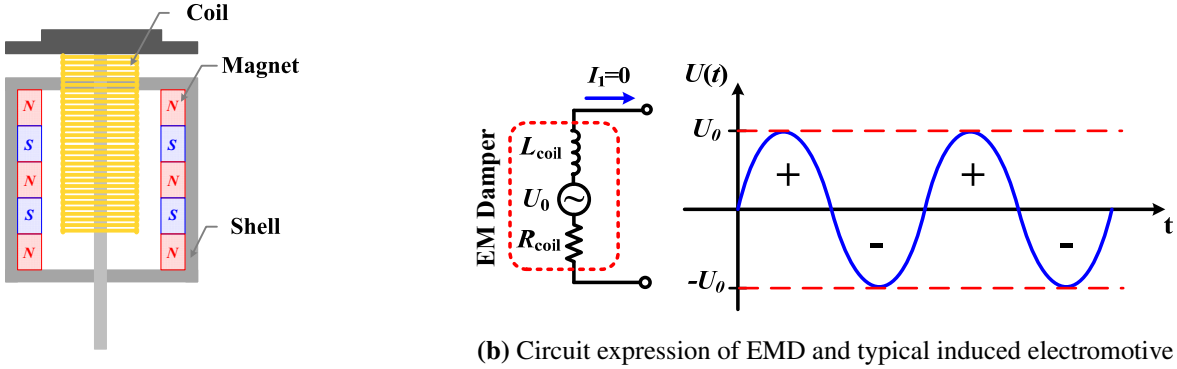

(a) Electromagnetic damper (LVCM)

(b) Circuit expression of EMD and typical induced electromotive force

FIGURE 3 Electromagnetic damper (EMD) device with typical generated voltage

The EMD can be shown as an electrical open circuit. To use the induced current, the EMD circuit needs to be closed. In this work, several resistors are first selected to cascade with the EMD as shown in Figures 4 a and 4 b. Next, the shunt circuit is replaced with an RLC circuit as shown in Figures 4 c and 4 d.

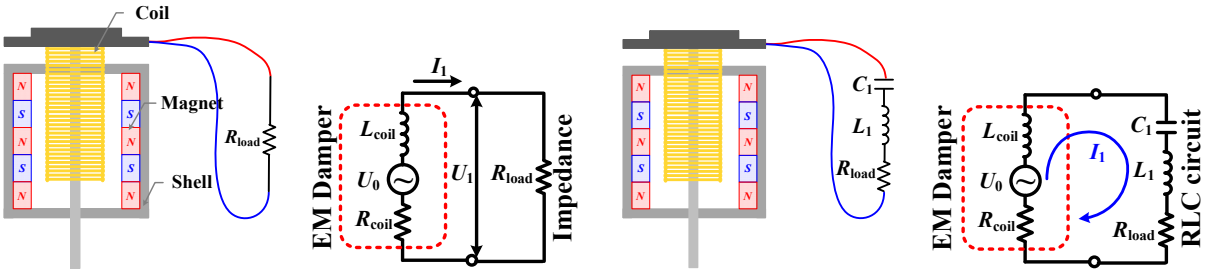

(a) EMD (LVCM) with impedance

(b) Circuit expression of EMD with impedance

(c) EMD (LVCM) with RLC circuit

(d) Circuit expression of EMD with RLC circuit

FIGURE 4 Electromagnetic damper (EMD) device with impedance and RLC shunt circuits

To perform an analytical study of the EMSD, an impedance shunt circuit is assumed to be connected to an EMD engaging the primary structure as shown in Figure 5 a. The governing equation is as follows:

$$\begin{bmatrix} m_1 & 0 \\ 0 & L_{coil} \end{bmatrix} \begin{Bmatrix} \ddot{x}_1 \\ \ddot{q} \end{Bmatrix} + \begin{bmatrix} c_1 & K_{emN} \\ -K_{emV} & R_{coil} + R_{load} \end{bmatrix} \begin{Bmatrix} \dot{x}_1 \\ q \end{Bmatrix} + \begin{bmatrix} k_1 & 0 \\ 0 & 0 \end{bmatrix} \begin{Bmatrix} x_1 \\ q \end{Bmatrix} = \begin{Bmatrix} f \\ 0 \end{Bmatrix} \tag{10}$$

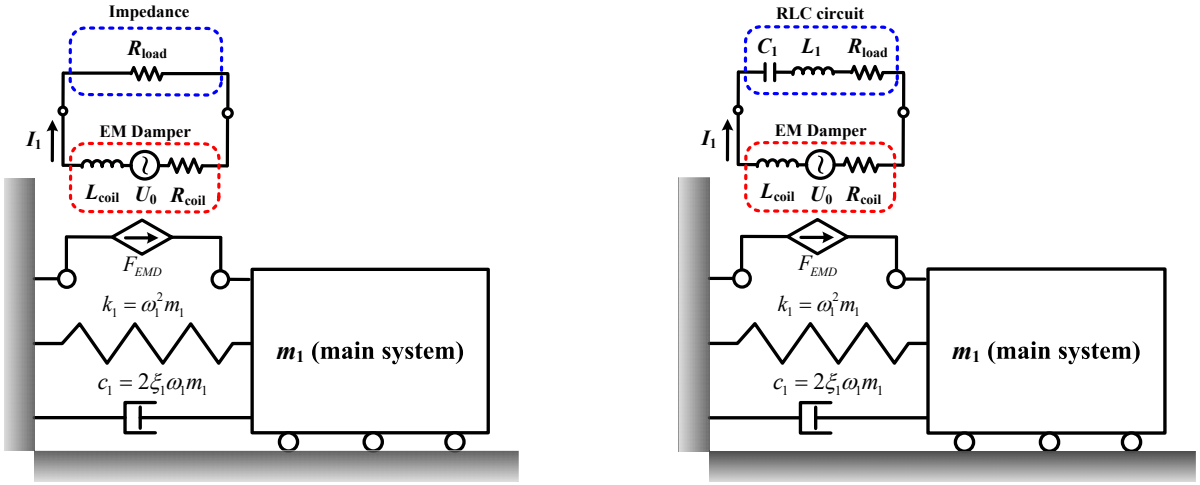

(a) SDOF system with EMSD (connecting with impedance)

(b) SDOF system with EMSD (connecting with RLC)

FIGURE 5 Electromagnetic damper (EMD) device

where R_{coil} and L_{coil} are the resistance and inductance of the EMD. K_{emN} is a machine constant of EMD, which is converted the induced current into electromagnetic force. K_{emV} is another machine constant of EMD, which is converted the relative velocity into emf. q is a electric charge. It is noted that using the concept of the series-parallel circuit, the total resistance $R_{coil} + R_{load}$ can be expressed as R, to simplify the equation. Taking the Laplace transform, the transfer function of the SDOF system with EMSD (impedance shunt circuit) can be written as follows:

$$\frac{X(s)}{F(s)} = \frac{sL + R}{s^3 m_1 L + \left(m_1 R + c_1 L\right) s^2 + \left(c_1 R + k_1 L + K_{emN} K_{emV}\right) s + k_1 R} \tag{11}$$

However, the shunt circuit might also be an RLC circuit. Figure 4 c shows the conceptual diagram of the EMD connected to an RLC circuit and Figure 4 d shows its circuit expression. Figure 5 b shows this type of EMSD setup in the horizontal direction. The governing equations can be derived as follows:

$$\begin{bmatrix} m_1 & 0 \\ 0 & L_{coil}+L_1 \end{bmatrix} \begin{Bmatrix} \ddot{x}_1 \\ \ddot{q} \end{Bmatrix} + \begin{bmatrix} c_1 & K_{emN} \\ -K_{emV} & R_{coil}+R_1 \end{bmatrix} \begin{Bmatrix} \dot{x}_1 \\ \dot{q} \end{Bmatrix} + \begin{bmatrix} k_1 & 0 \\ 0 & \frac{1}{C_1} \end{bmatrix} \begin{Bmatrix} x_1 \\ q \end{Bmatrix} = \begin{Bmatrix} f \\ 0 \end{Bmatrix} \tag{12}$$

To acquire the dynamic response of the EMSD system, the corresponding Laplace transformation result is shown as

$$\frac{X_1(s)}{F(s)} = \frac{s^2L + sR + \frac{1}{C}}{s^4 m_1 L + \left(m_1 R + c_1 L\right) s^3 + \left(\frac{m_1}{C} + c_1 R + k_1 L + K_{emN}K_{emV}\right) s^2 + \left(\frac{c_1}{C} + Rk_1\right) s + \frac{k_1}{C}} \tag{13}$$

From a basic RLC oscillating circuit, it is noted that the natural frequency of the RLC circuit can stand for $\omega_{2,eq} = \sqrt{\frac{1}{LC}}$ and the damping ratio (damping factor) can be represented as $\xi_{2,eq} = \frac{R}{2}\sqrt{\frac{C}{L}}$. From this point of view, equation 13 can be rewritten as follows:

$$\frac{X_1(s)}{F(s)} = \frac{s^2 + 2\xi_{2,eq}\omega_{2,eq}s + {\omega_{2,eq}}^2}{m_1 s^4 + \left(m_1\frac{R}{L} + c_1\right) s^3 + \left(m_1{\omega_{2,eq}}^2 + c_1\frac{R}{L} + k_1 + \frac{K_{emN}K_{emV}}{L}\right) s^2 + \left(c_1{\omega_{2,eq}}^2 + k_1\frac{R}{L}\right) s + k_1{\omega_{2,eq}}^2} \tag{14}$$

In equations 11 and 13, to make the further calculation simple, C, L and R represent total values of capacitor, inductor and resistor.

Meanwhile, papers [37] and [2, 3] observed that the EMD with RLC circuit transfer function can have a coincidental form as equation 5; therefore, the equivalent mass ratio $\mu_{eq} = \frac{m_{2,eq}}{m_1}$ and the equivalent frequency ratios can then be defined as $\gamma_{eq} = \frac{\omega_{2,eq}}{\omega_1}$, in which $m_{2,eq} = K_{emN}K_{emV}C$ is equivalent mass (virtual mass). The equation 14 can be rewritten as:

$$G_{eq}(\lambda) = \frac{X_1(\lambda)}{F(\lambda)/k_1} = \frac{{\gamma_{eq}}^2 - \lambda^2 + j2\xi_{2,eq}\gamma_{eq}\lambda}{\lambda^4 + {\gamma_{eq}}^2 - {\gamma_{eq}}^2\lambda^2 - \lambda^2 - \mu_{eq}{\gamma_{eq}}^2\lambda^2 + j\left(-2\xi_{2.eq}\gamma_{eq}\lambda^3 + 2\xi_{2,eq}\gamma_{eq}\lambda\right)} \tag{15}$$

Performing robust optimisation design of the EMDS (RLC) system, the H_∞ mathematical model can reference to [37]. As a result, the optimal frequency ratio and damping ratio under H_∞ design can be expressed as:

$$\gamma_{opt,eq} = \sqrt{\frac{2}{2+\mu_{eq}}} \tag{16}$$

$$\xi_{2,eq,opt} = \sqrt{\frac{3\mu_{eq}}{8}} \tag{17}$$

Otherwise, [2, 3] proposes another common use H_2 robust optimisation control method. The corresponding frequency and damping ratio can be shown as:

$$\xi_{2,eq,opt} = \frac{1}{2}\sqrt{{\gamma_{eq}}^2 + \mu_{eq}{\gamma_{eq}}^2 - 2 + \frac{1}{{\gamma_{eq}}^2}} \tag{18}$$

$$\gamma_{eq,opt} = 1 \tag{19}$$

Papers [37, 2, 3] were given the equivalent peak dynamic amplification factor of EMSD design under H_∞ optimisation, which can be written as follows:

$$G_{opt,eq} = \sqrt{\frac{2+\mu_{eq}}{\mu_{eq}}} \tag{20}$$

where the $G_{opt,eq}$ can be depicted by equivalent mass ratio. Figure 6 shows a plot to describe the equivalent peak dynamic amplification factor varied by equivalent mass ratio and capacitance. It can be seen that a higher equivalent mass ratio is to have higher capacitance and induce a lower magnitude of the peak amplification factor. This shows the fact that a large mass ratio can reduce more dynamic response. In Figure 6 , black triangle marker is the further study (section 7.2) selected mass ratio (0.08 %), indeed.

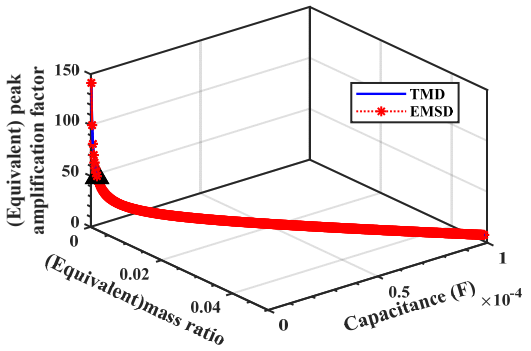

FIGURE 6 Equivalent peak amplification factor under H_∞ optimisation with μ =0.08%

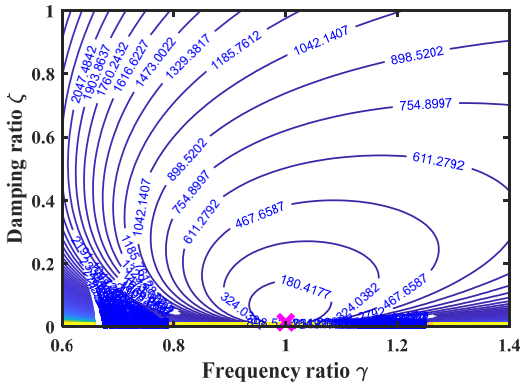

FIGURE 7 Dimensionless mean square function under H_2 optimisation with μ =0.08%

On the other hand, the correlated mean square objective function under H_2 optimisation is given by papers [2, 3], which is noted as follows:

$$E\left[\left|G(\lambda)^2\right|\right] = \pi\omega_n S_0 \frac{\gamma_{eq}^4 + \mu_{eq}\gamma_{eq}^4 + 4\zeta_{2,eq}^2\gamma_{eq}^2 - 2\gamma_{eq}^2 + 1}{2\zeta_{2.eq}\mu_{eq}\gamma_{eq}^3} \tag{21}$$

By substituting equations 18 and 19 into equation 21, Figure 7 shows a contour of the dimensionless mean square objective function under H_2 optimisation. The cross marker in Figure 7 illustrates a global minimum value when the correlated mass ratio in 0.08 %. Then the correlated optimal damping and frequency ratios will be confirmed.

Both robust optimisation methods were showed that the two types of optimal design ratios are a function of the equivalent mass ratio.

The use of EMSD uses in controlling civil building structure dynamics has had many unknowns and limitations. As a result, in this paper, the first step is to determine whether the EMSD is capable of overcoming and dealing with vibration suppression. Therefore, the shunt circuits (R series and RLC) are chosen to apply to the system. The following section discusses the EMSD application and performs the relative testing on the MRF structure.

4 | DESCRIPTION OF THE LINEAR VOICE COIL MOTOR

For the purpose of this study, an EMD - Linear Voice Coil Motor (LVCM) GVCM- 095-089-01S06 (by Moticont) was selected, as shown in Figure 8 . This kind of electromagnetic actuator is widely used in industrial production lines, whereas it is used here as an EMD. This EMD contains three main components: the outside shell of the motor containing ring magnets, the copper coil in the middle, and a permanent magnet mounted at the core of the shell case.

The copper coil is a conductive material. According to electromagnetic induction theory, changing the magnetic flux or cutting through the magnetic lines within the magnetic density field represents a relative motion between the magnet and conductor. The Eddy current (induced current) and induced electromotive force (emf) can thus be generated.

Table 1 shows some significant data regarding the LVCM. The previous studies from [37] and [2] mentioned two machine constants (force constant and back emf constant) required in the design of the EMSD. The force constant K_{emN} is expressed as current converted to force, while the back emf constant K_{emV} represents velocity converted to voltage. The selected LVCM has equal values for these two machine constants, 22.2 N/A and 22.2 V/(m/s), respectively.

The electromagnetic LVCM in this study is used for electromagnetic damping. The EMD force is proportional to the induced current, whereas the induced voltage is proportional to the system velocity, as proven by [2]. The other properties of the LVCM such as inherent resistance and coil inductance used in the EMSD design process are 3 Ω and 2.1 mH, respectively.

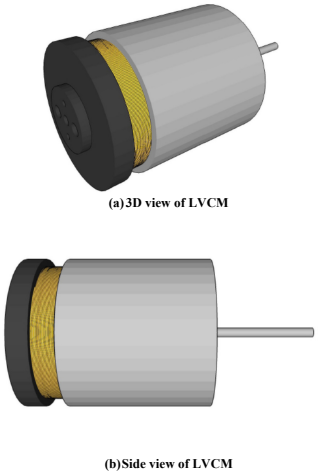

FIGURE 8 Electromagnetic linear voice coil motor

Intermittent force 10% duty cycle	351.1 (N)
Continuous force	111.2 (N)
Force constant	22.2 (N/A)
Back EMF constant	22.2 (V/(m/s))
Stroke	63.5 (mm)
Body Mass	4.1 (kg)
Coil resistance	3 (Ohms)
Coil inductance	2.1 (mH)

TABLE 1 Technical characteristics of Linear Voice Coil Motor (source: adapted from Moticont catalogue - Linear Voice Coil Motor)

5 | ALUMINIUM MOMENT RESISTING FRAME (AMRF) WITH EMD

The EMD was positioned on the second level of the AMRF structure, as shown in Figure 9 . However, the weight of the EMD and its mountings also add to the structural mass, which might change the structural properties and affect the EMSD design. To monitor this change, the physical model was retested to identify the updated dynamic properties of the structure.

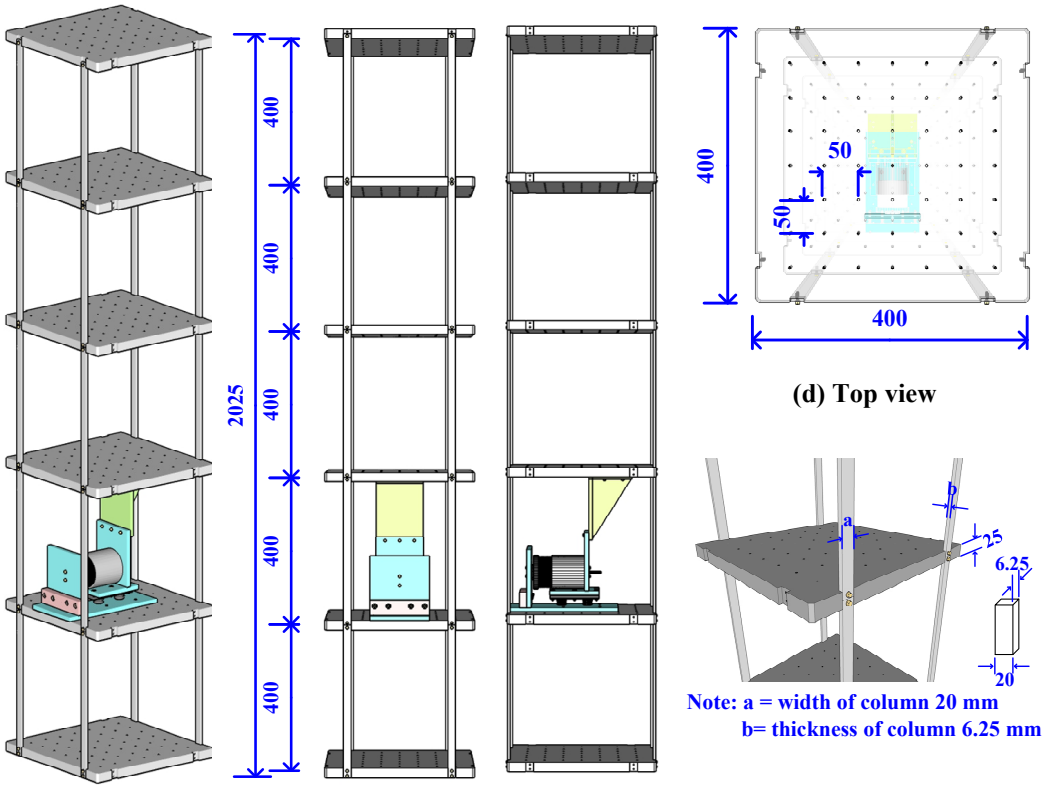

FIGURE 9 Diagram of AMRF with LVCM at 2F

In this work, the EMSD was used for passive control. The activation of the EMD relies on relative motion between the conductive coil and the magnets. The conductive coil is attached to the second level of the AMRF, while the magnet is attached to the underside of the third level. Figure 10 shows the mounting arrangement. Therefore, when the shear motion occurs in the AMRF, the LVCM is activated and moved by the relative movement of the second-third level in one direction.

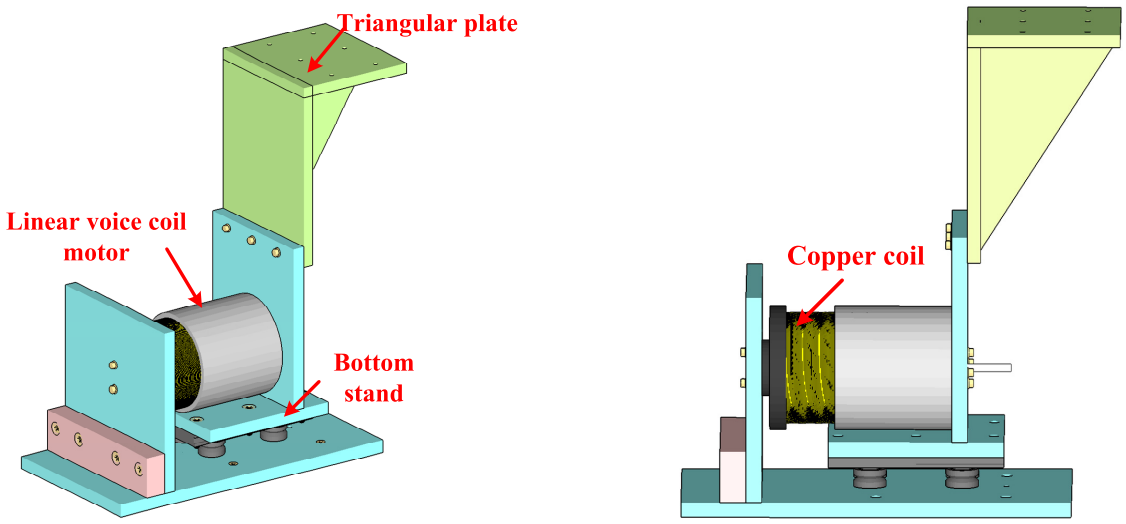

(a) 3D view **(b)** Side view

FIGURE 10 LVCM with mounting stand

5.1 | Data acquisition devices and excitation source

Modal testing was used to obtain the structural properties using a range of sensors. This section introduces the sensors used and their setup in the AMRF-EMSD system.

Figure 11 a shows all the sensors and the LVCM setup. Six Endevco7754A-1000 accelerometers, an ImetrumISM-VG4-PRO optical displacement measurement system, and two MTS Model RH-M-0150M-060-1-A01 magnetostrictive position sensors were used to measure the acceleration and displacement responses.

In this study, the Imetrum device was used for measuring the horizontal and vertical displacement on each level, whereas the MTS sensors were only mounted on the second and third floors, for monitoring the damper. Using two different types of sensors gave a mechanism to verify the measured data accuracy.

The Endevco accelerometers were set up in the horizontal direction on each level, parallel to the MTS sensors. These gave a third method to verify the response of the structure.

The chosen excitation source was an APS Dynamics Inc. Model 400 electro-sei shaker, as shown in Figure 12 a, connected to the underside of the second level via a rigid bar. Two load cells were connected between the APS shaker and the rigid bar, and the LVCM and the mounting stand. Entran ELPM-T3M-1.25kN tension and compression type load cells were chosen. The measured range of the load cell is within $\pm$1250 N.

5.2 | Modal testing of AMRF with disconnected LVCM

Figure 12 a shows a photo of the testing setup. A small column was built for mounting the MTS sensors at the second and third level, and the magnet rings were mounted on the AMRF.

Figure 12 b shows the disconnected EMD. The coil core is separate from the magnet, but the weight is still contributing to that of the second floor. The magnet tube is connected to the bottom of the third floor via the triangular plate. From this point of view, the mass source does not change in case of connecting or disconnecting the LVCM.

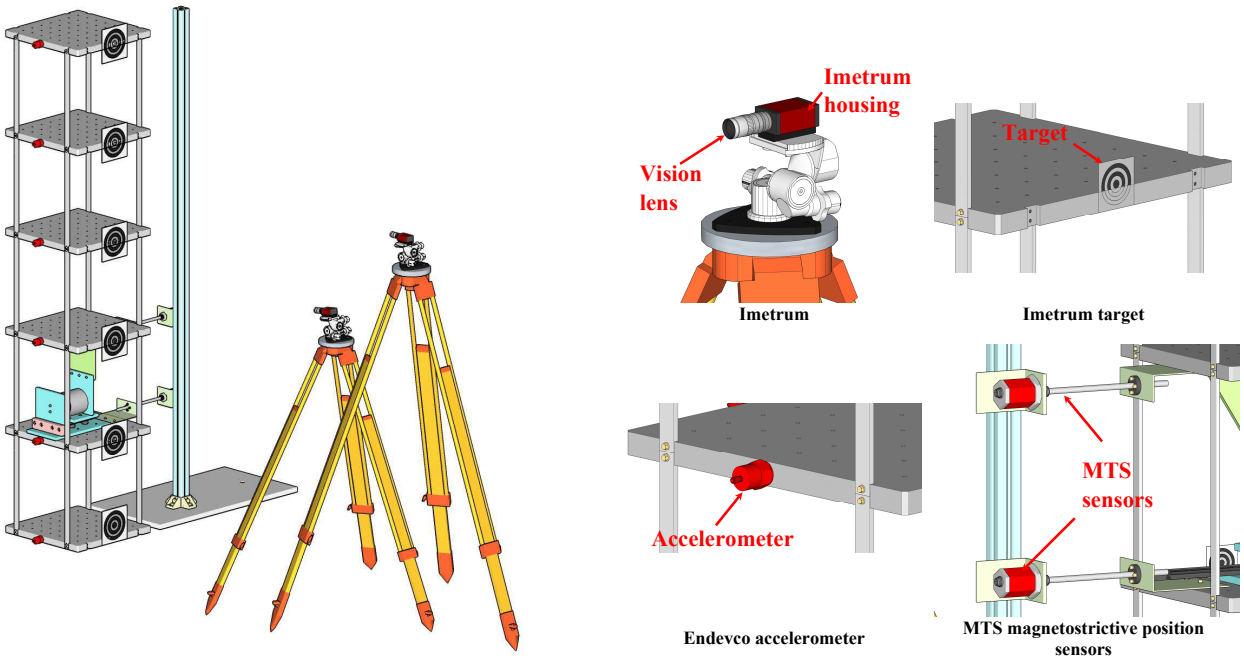

(a) 3D view of setup **(b)** All data acquisition sensors

FIGURE 11 Aluminium frame with LVCM and all sensors

Once the experimental setup was ready, a random signal was selected to excite the structure. Figure 13 a shows the measured frequency response functions (FRFs). The frequency span selected was 0-20 Hz. From the FRFs, it can be seen that the first mode frequency is around 1.5-2.0 Hz. The phase angle is also shown in Figure 13 b, which varies between -180 and 180 degrees and has negative phase shifts through modes.

Table 2 shows the first five measured natural frequencies, damping ratio and modal mass, together with the FE calculated natural frequencies. The first mode has a frequency of 1.81 Hz, damping ratio of 0.33 % and modal mass of 36.59 kg. This first mode will be used to perform the design of the EMSD.

Mode Number	Measured natural Frequency (Hz)	Damping Ratio (%)	Modal Mass (kg)
1	1.81	0.33	36.59
2	4.83	0.35	41.97
3	8.00	0.36	37.64
4	9.86	0.27	74.68
5	12.87	0.18	21.59

TABLE 2 Measured dynamic properties of the six-storey aluminium AMRF with disconnected LVCM at 2F

The measured mode shapes of the structure are shown in Figure 14 . The orange dot of the measured mode shape diagram represents the excitation input location, which is on the second floor.

Using the measured properties, the result of the FRF curve-fit of the second level is shown in Figure 15 . The curve-fitting indicates a satisfactory numerical approximation of the structural dynamics. The modal properties will be used to implement the design process of the EMSD in the next section.

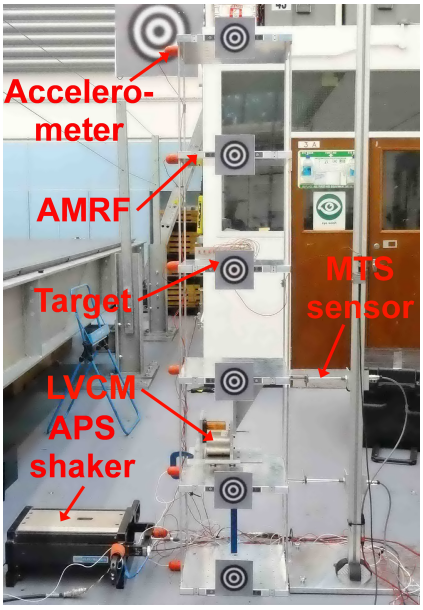

(a) Photo of AMRF with disconnected LVCM

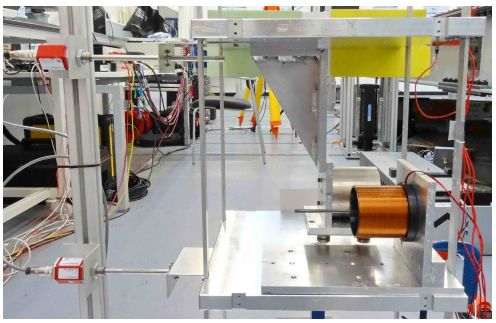

(b) Photo zoom in of AMRF with disconnected LVCM

FIGURE 12 Photo of the AMRF with LVCM

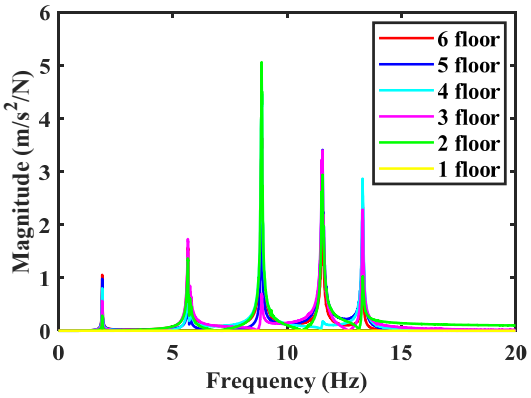

(a) FRF magnitude

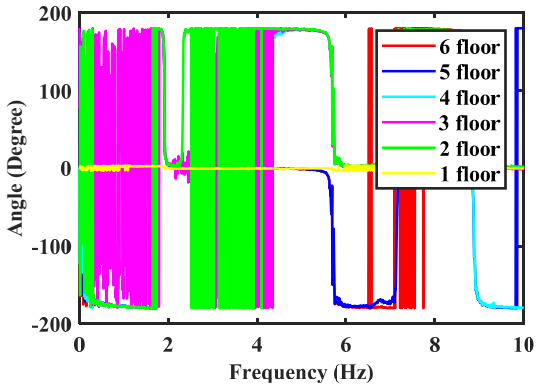

(b) FRF phase

FIGURE 13 Dynamic response of AMRF with disconnected LVCM at 2F

5.3 | Design methodology of two categories EMSD

For performing the EMSD design to multi-degree-of-freedom (MDOF) system, the concept of the mode decomposition method [14, 13] is necessary to introduce in this subsection. The mode decomposition method is the use of system eigenmode vector to transform the simultaneous equations of the MDOF system into a series of independent equations with only one variable. These independent equations with only one variable are essentially multiple equations of motion of single-degree-of-freedom (SDOF) system. In this way, each SDOF system response can be solved conveniently. Finally, applying the superposition technique to the response of these SDOF systems, the final response of the original MDOF structure is to be achieved. Therefore, the mode decomposition method is used for MDOF system.

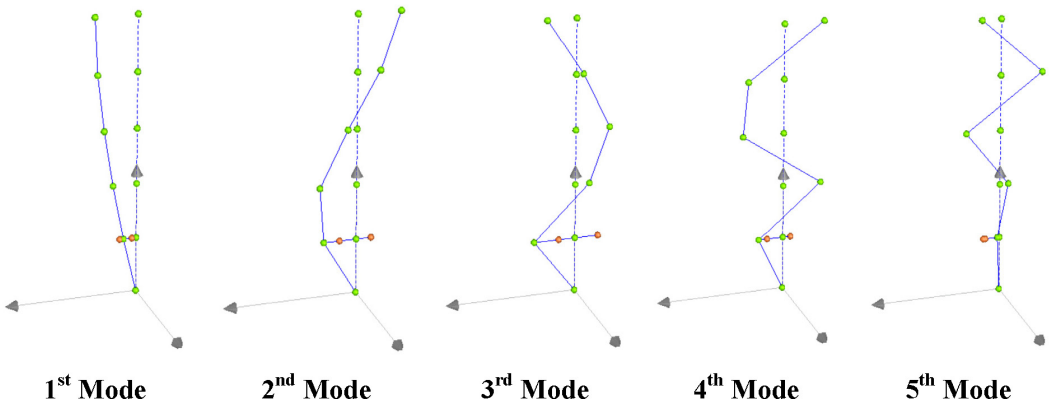

FIGURE 14 Mode shapes of AMRF with disconnected LVCM at 2F

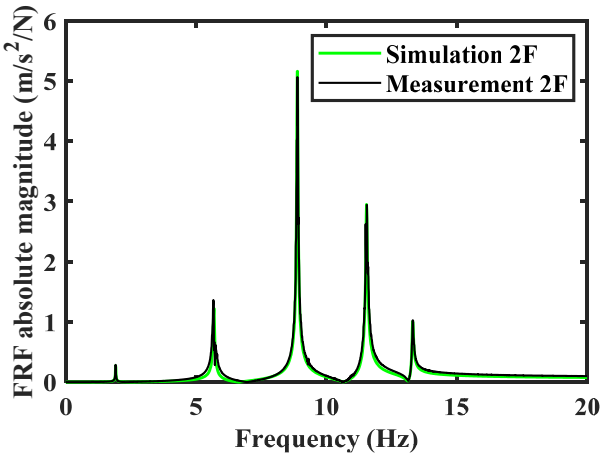

FIGURE 15 Curve-fitting of AMRF with disconnected LVCM at 2F

In a linear MDOF system, the equation of motion can be written as:

$$\boldsymbol{M}\ddot{\boldsymbol{X}} + \boldsymbol{C}\dot{\boldsymbol{X}} + \boldsymbol{K}\boldsymbol{X} = \boldsymbol{F}(\boldsymbol{t}) \tag{22}$$

where $\boldsymbol{M}$, $\boldsymbol{C}$ and $\boldsymbol{K}$ are system mass, damping and stiffness matrices. $\boldsymbol{F}$ is the excitation matrix. The mode shapes of free vibration $\boldsymbol{\Phi}$ is a method of representing displacement, and these mode shapes constitute n independent displacement matrix, for any displacements $\boldsymbol{X} = \boldsymbol{\Phi}\boldsymbol{Z} = \sum_{i=1}^{n} \boldsymbol{\Phi}_i Z_i$, then substituting into the equation 22, which is given by:

$$\boldsymbol{M}\boldsymbol{\Phi}\ddot{\boldsymbol{Z}} + \boldsymbol{C}\boldsymbol{\Phi}\dot{\boldsymbol{Z}} + \boldsymbol{K}\boldsymbol{\Phi}\boldsymbol{Z} = \boldsymbol{F}(\boldsymbol{t}) \tag{23}$$

Multiplying $\boldsymbol{\Phi}^T$ on both sides of the equation 23 and applying the mode shapes orthogonality to mass and stiffness matrices, then the equation of motion can be rewritten as:

$$\boldsymbol{M}^*\ddot{\boldsymbol{Z}} + \boldsymbol{C}^*\dot{\boldsymbol{Z}} + \boldsymbol{K}^*\boldsymbol{Z} = \boldsymbol{F}^*(\boldsymbol{t}) \tag{24}$$

where $\boldsymbol{M}^*$, $\boldsymbol{C}^*$ and $\boldsymbol{K}^*$ are diagonal matrices, $M_i^* = \boldsymbol{\Phi}_i^T \boldsymbol{M} \boldsymbol{\Phi}_i$, $C_i^* = \boldsymbol{\Phi}_i^T \boldsymbol{C} \boldsymbol{\Phi}_i$, $K_i^* = \boldsymbol{\Phi}_i^T \boldsymbol{K} \boldsymbol{\Phi}_i$, $F_i^*(t) = \boldsymbol{\Phi}_i^T \boldsymbol{F}(\boldsymbol{t})$. Hence, the simultaneous motion equation of a MDOF system can be completely transformed into multiple SDOF equations of motion, which is given by:

$$M_i^*\ddot{Z}_i + C_i^*\dot{Z}_i + K_i^* Z_i = F_i^*(t) \qquad (i = 1, \cdots n) \tag{25}$$

By using the equation 25 and the results of model testing in subsection 5.2, Figure 16 is shown the second floor FRF and regenerated FRF based on the measured data, measured FRF and mode decomposition estimation.

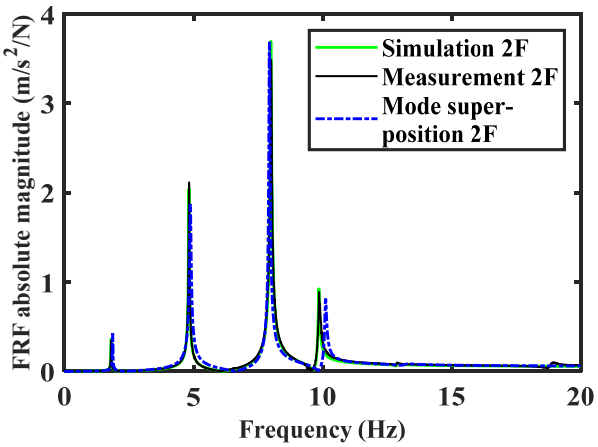

FIGURE 16 Mode decomposition method curve fitting of AMRF with disconnected LVCM at 2F

From this point of view, the mode decomposition estimated FRF curve has almost consistent result as the measured FRF. Consequently, the mode decomposition method is effectively applied to the MDOF system and used to calculate the mode shapes analytically.

5.3.1 | Design methodology of EMSD using impedance shunt circuit

Using structure mode shapes from the results of the modal testing or mathematical modal analysis to calculate the sum of the work of all dampers and find out the corresponding elastic strain energy. The effective damping ratio calculation of VDs can be easily extended from the SDOF to MDOF system.

The strain energy design method [18, 17] for viscous dampers was used for the calculation of the effective damping, as shown in equation 2. This method can also be applied to determine the equivalent damping ratio of the EMSD with impedance shunt circuit. The magnitude of induced voltage can be calculated by multiplying the voltage machine constant and velocity, as shown in equations 10 and 12. The resultant electromagnetic force is presented as follows [2]:

$$F_{emN} = F_{em,total} = K_{emN} i \tag{26}$$

Through the use of Ohm's law, it is not difficult to determine that the updated resultant EMSD damping force can be expressed by two machine constants and resistance, as follows:

$$\boldsymbol{F_{emN}} = \frac{K_{emN} K_{emV}}{R} \dot{\boldsymbol{x}} \tag{27}$$

From the above equation, it can be seen that the updated resultant EMSD damping force is also proportional to the velocity. When compared with the viscous damping force in equation 1 it can be seen that they have a similar expression. Based on this, the equivalent damping coefficient of the EMSD with impedance shunt circuit can be expressed as follows:

$$C_{eq} = \frac{K_{emN} K_{emV}}{R} \tag{28}$$

To calculate the equivalent damping ratio of the EMSD with impedance shunt circuit, equation 28 is used instead of C_j of equation 2. Hence, the equivalent damping ratio can be rewritten as follows:

$$\zeta_{eq,EMSD,R} = \frac{T_n \sum_i C_{eq,i} \left(\phi_{ri} \cos\theta_i\right)^2}{4\pi \sum_j m_j \phi_j^2} = \frac{T_n \sum_i \frac{K_{emN,i} K_{emV,i}}{R_i} \left(\phi_{ri} \cos\theta_i\right)^2}{4\pi \sum_j m_j \phi_j^2} \tag{29}$$

Once the structural properties were confirmed, the equivalent damping ratio is proportional to the coefficient of $\frac{K_{emN} K_{emV}}{R}$. Also, when the LVCM selected, machine constants will not change; therefore, the equivalent damping ratio is inverse proportion to resistance R. Based on the design purpose, in this study wants to add additional 1.35 % damping to improve the structure dynamics. Using the equation 29, the resistor can be determined to the value of 0.3 Ω for the shunt circuit design. Otherwise, this study also selected different resistors to verify the EMSD concept, which will be discussed in subsection 6.1.

5.3.2 | Design methodology of EMSD using RLC shunt circuit

When the LVCM parameters were found, equations 16 and 17 (H_∞ optimisation) and equations 18 and 19 (H_2 optimisation) can be used for determining optimal damping and frequency ratios for EMSD using RLC shunt circuit, but these equations are only applicable to SDOF system. Most structures are MDOF systems, so a more general form is needed to describe the dynamic behavior of a structural system during subjected to external excitation. In previous content of this section was mentioned the mode decomposition method. This could apply to the design of the EMSD (RLC shunt circuit) in MDOF system. Substituting of mass, stiffness and damping into modal mass, modal stiffness and modal damping, then the equivalent mass ratio for MDOF system can be rewritten as:

$$\mu_{eq}^{*} = \frac{m_{2,eq}}{M_{i}^{*}} \tag{30}$$

In this study, the first mode of the structure dynamics is selected to verify the vibration suppression; therefore, the M_i^* of the equation 30 can replace to M_1^*, in which 1 represents the first mode. Also, to select the correlated EMSD RLC optimal circuit components for H_∞ and H_2 optimisation, the proposed formulae from papers [2, 3] need to be rewritten as follows:

	H_∞ optimisation	H_2 optimisation
Optimal resistnace R_{opt}^{*}	$\sqrt{\frac{3}{2}\frac{K_{emN}K_{emV}L_{opt}}{M_1^*}}$	$\sqrt{\frac{\mu_{eq}^{*}L_{opt}^{*}}{C}}$
Optimal inductance L_{opt}^{*}	$\frac{K_{emN}K_{emV}\left(2M_1^*+m_{2.eq}\right)}{2m_{2,eq}K_1^*}$	$\frac{K_{emN}K_{emV}}{m_{2,eq}\omega_1^2}$

TABLE 3 RLC optimal circuit components design formulae of the EMSD using H_∞ and H_2

From the section 3 can be known that the equivalent mass is a function of capacitance. When the capacitance value is determined, the other components will be confirmed. It can be seen that the capacitance is the main design influence parameter.

6 | EXPERIMENTAL VALIDATION

This section presents experimental studies of R and RLC shunt circuits applied to the AMRF structure to evaluate their performance in light of the previous analytical studies. Figure 17 shows the LVCM set up between the second and third levels. The conductive coil is now located inside the magnet tube and the displacement of the coil relative to the magnets is equal to the difference in displacement between the second and third floors.

6.1 | EMSD using impedance shunt circuit

In the first set of experiments, the LVCM (EMD) coil is connected in turn to a number of different impedance circuits, as shown in Figure 18 a. The values of the resistors selected are 0.3 Ω (original design), 5.6 Ω, 10 Ω, 22 Ω, 39 Ω and 1000 Ω. The inherent resistance of the EMD coil is 3 Ω. This means that the total resistance is the sum of the shunt and inherent resistances together.

Figures 19 and 20 show the FRFs between the excitation and the second and sixth levels under a random excitation signal. The disconnected LVCM is included where the conductive coil and magnet tube are disconnected. The open circuit represents the case where the LVCM is connected, but the terminals are not connected to a shunt circuit. The closed circuit refers to the case where the terminals are directly connected to each other without a shunt circuit.

From the FRF curves, the lower resistances demonstrate a better reduction, particularly in the case of the closed circuit. The highest value of the resistance, 1000 Ω in this study, has almost no damping effect. From the FRF responses, it can be seen that the EMSD with impedance shunt circuit increases the system damping in a manner which is dependent on the shunt resistance.

The mode shapes of the structure with the LVCM installed with the 0.3 Ω impedance shunt circuit are shown in Figure 21 . It is noted that the different shunt circuits tested have a similar mode shapes.

A chirp signal was selected next to excite the system. This input sweeps through a range from 1.5-2.5 Hz, to cover the first mode of vibration.

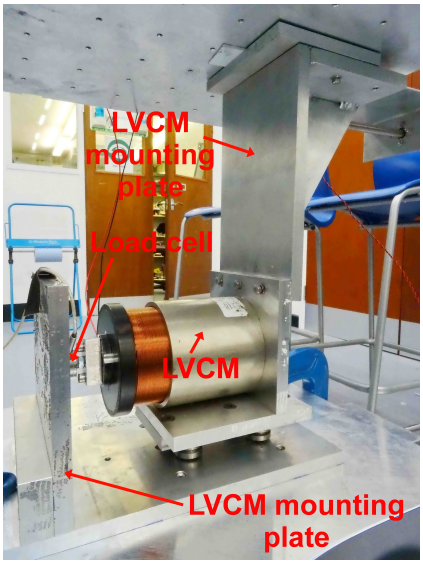

FIGURE 17 Photo of AMRF with LVCM connected

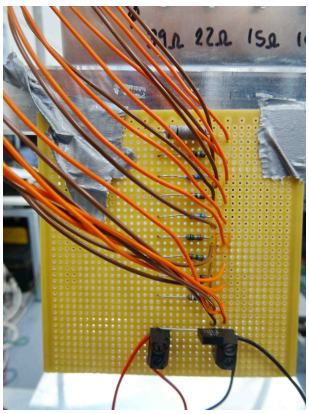

(a) Photo of impedance series circuit

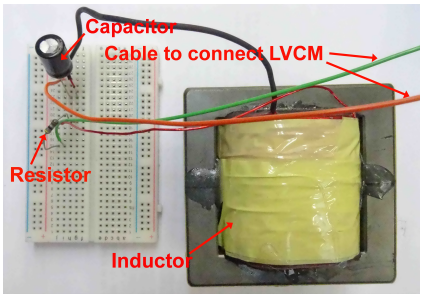

(b) Photo of RLC circuit

FIGURE 18 Photo of the impedance series circuit, H_∞ and H_2 RLC circuits

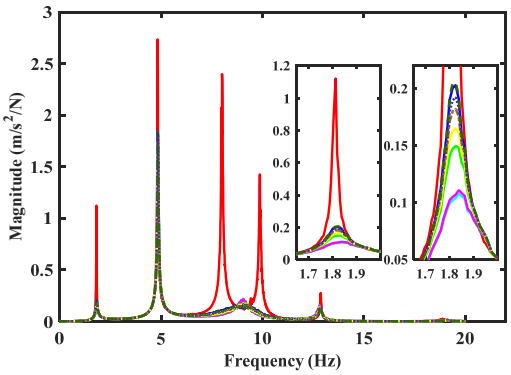

(a) FRF magnitude

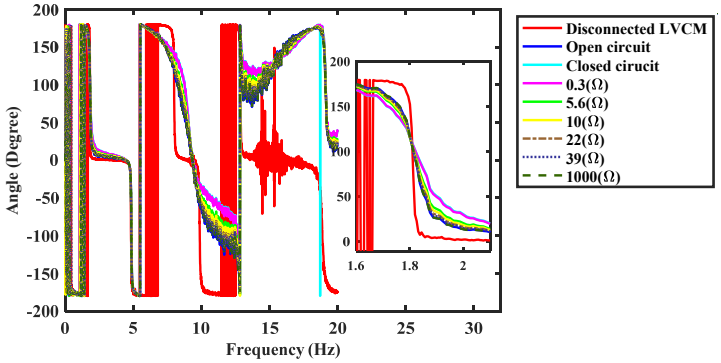

(b) FRF phase

FIGURE 19 Sixth floor FRFs of AMRF with EMSD connected and using different shunt impedance circuits

Figure 22 shows the FRF curves at the sixth and second levels under the chirp signal input. These results also show that better damping effect is achieved for lower resistances.

The purpose of the EMSD system is to generate electromotive force (emf) via electromagnetic induction, and then the induced current can be retrieved flowing through a shunt circuit to provide a damping effect to the system. The different shunt circuits provide different damping effects (or filtering effects). The emf time history is shown in Figure 23 for the range of impedance circuits tested.

The generated emf relies on the relative motion between the conductive coil and magnet tube, i.e. on the storey shear motion. From Figure 23 it can be seen that the 1000 Ω resistance produces the highest induced emf, whereas the 0.3 Ω resistance produces a lower induced emf. For each value of resistance, the induced current is given by $I = \frac{V}{R}$, i.e. the emf divided by the resistance of the shunt circuit and LVCM together. Time histories of the induced currents are shown in Figure 24 for the various shunt circuits.

Since the damping force is a function of the induced current, it is expected that higher currents will result in higher damping forces. This is evident from Figure 25 which shows greater damping force from the 0.3 Ω shunt circuit than the 1000 Ω shunt circuit. It is noted that the EMSD using a 0.3 Ω for the shunt circuit has a damping force of approximately 20 N. This is associated with the requirements of dynamic behaviour control of the AMRF. In comparison with VD, a model 1x2D D-series

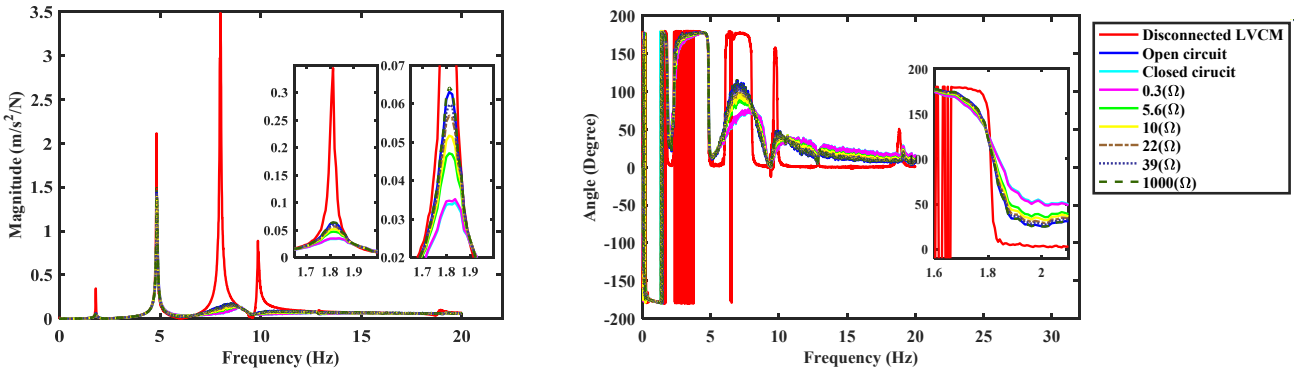

(a) FRF magnitude **(b)** FRF phase

FIGURE 20 Second floor FRFs of AMRF with EMSD connected and using different shunt impedance circuits

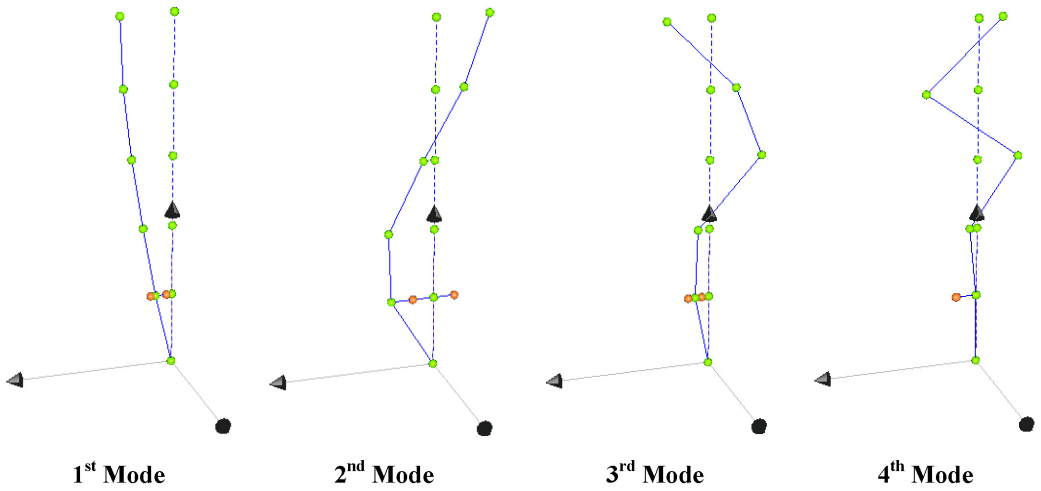

FIGURE 21 Mode shape of AMRF with LVCM (0.3 Ω shunt circuit) between 2F and 3F

linear damper of the Taylor devices inc. [1] (smallest size specification) could use to compare, which dimension fits the space between 2nd and 3rd floors and has output force in 2000 N. Indeed, a higher damping force could reduce more dynamic response. However, the damping value from VD is too high in this application, which does not meet the design requirement of adding 1.35 % additional damping. Also, this research is to find a feasible alternative solution to replace the traditional damping, so the EMSD impedance circuit was developed. From the results of the principle and experiment, the EMSD damping force can be enhanced as similar grade as VD by choosing higher machine constants, higher-grade magnet, a better electrical conductivity of the conductor and connect lower values of resistance or negative resistance, but the establishment of negative resistance is not included in this study.

To further compare the controlling effect of the EMSD with impedance shunt circuit, Figures 26 a and 26 b shows the peak acceleration and displacement for each level of the AMRF. Overall, the acceleration and displacement plots indicate that both experience a reduction following connection of the EMSD.

When compared with the disconnected LVCM, the closed circuit with lower resistance values (e.g. 0.3 Ω) produces a significant reduction in displacement and acceleration; approximately 63 % and 64 %, respectively. In this experimental study, the 1000 Ω resistance gives reductions of only 29 % for displacement and 31 % for acceleration. This is expected since the generated current is low.

Figure 26 c shows the inter-storey drift ratios comparison. It can be seen that the maximum drift ratio of the disconnected LVCM between the first and second and second and third levels are 4.95 % and 5.17 %. After the installation of the impedance

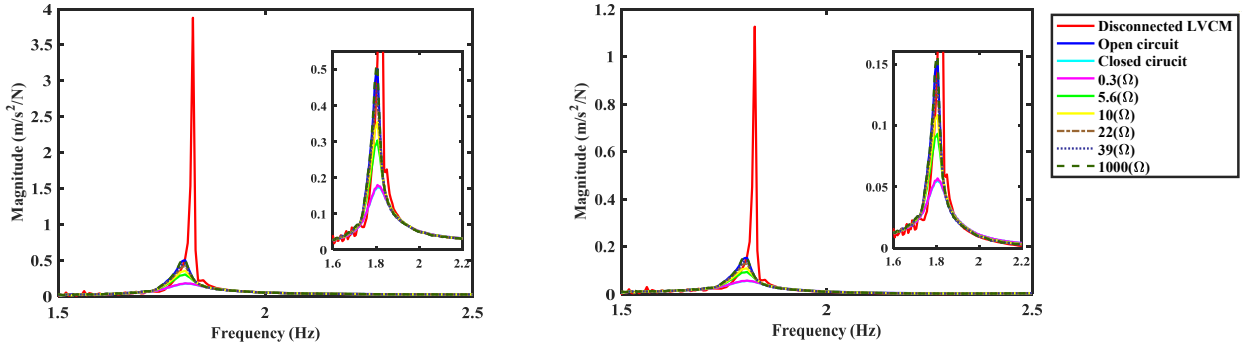

(a) 6F FRF curves **(b)** 2F FRF curves

FIGURE 22 Dynamic response under chirp signal input of AMRF with EMSD using different shunt impedance circuits

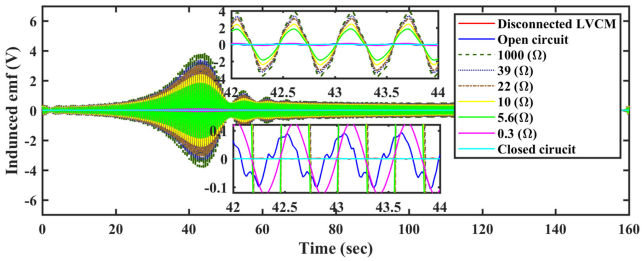

FIGURE 23 Induced emf time history under chirp signal input of AMRF with EMSD using different R shunt circuits

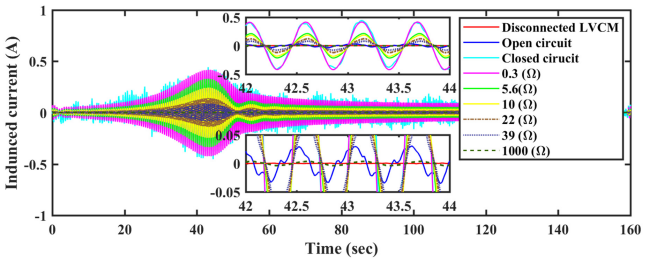

FIGURE 24 Induced current time history under chirp signal input of AMRF with EMSD using different R shunt circuits

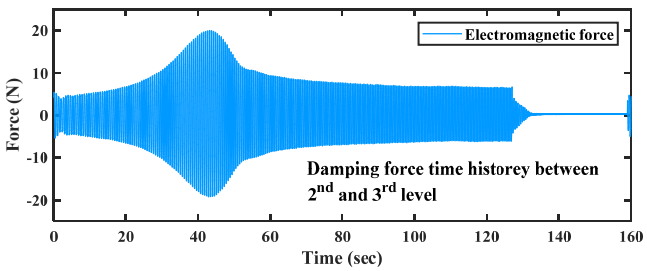

(a) 0.3 Ω shunt circuit

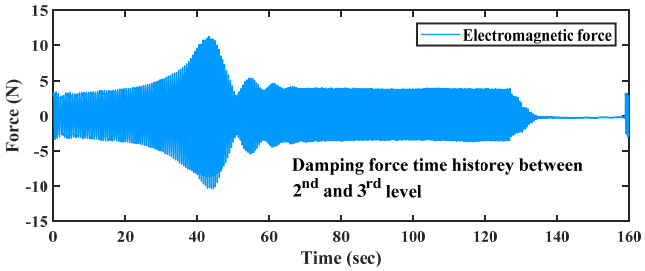

(b) 1000 Ω shunt circuit

FIGURE 25 The measured damping force time history of the EMSD using R shunt circuit

shunt circuits, the closed circuit is able to reduce the drift ratios to 1.998 % and 1.67 %, respectively. The 0.3 Ω resistance circuit results in a drift ratios of 1.98 % and 1.72 %, respectively. However, the 1000 Ω resistance circuit only produces 3.25 % and 3.85 %, respectively, which is relatively a small reduction.

Figures 27 , 28 and 29 show two types of different hysteresis loops. The first is the relation between damper force and displacement, and the other is the relation between damper force and induced voltage. If the damper behaves linearly, the relation of force and displacement is represented by a smooth elliptical shape. The force and induced voltage should have a linear proportional relationship.

The results of the hysteresis loops show that the shapes are not elliptical and linear, which suggests nonlinear behaviour is occurring in the system. It can be seen that the shape of the hysteresis loop in Figure 27 (tuned off EMSD) is close to 1000 Ω case, which represents the nonlinearity happened in the damper system itself. This nonlinearity might be due to different reasons. One possible cause might be friction; either friction between the coil and magnet assembly or air friction. From observation of

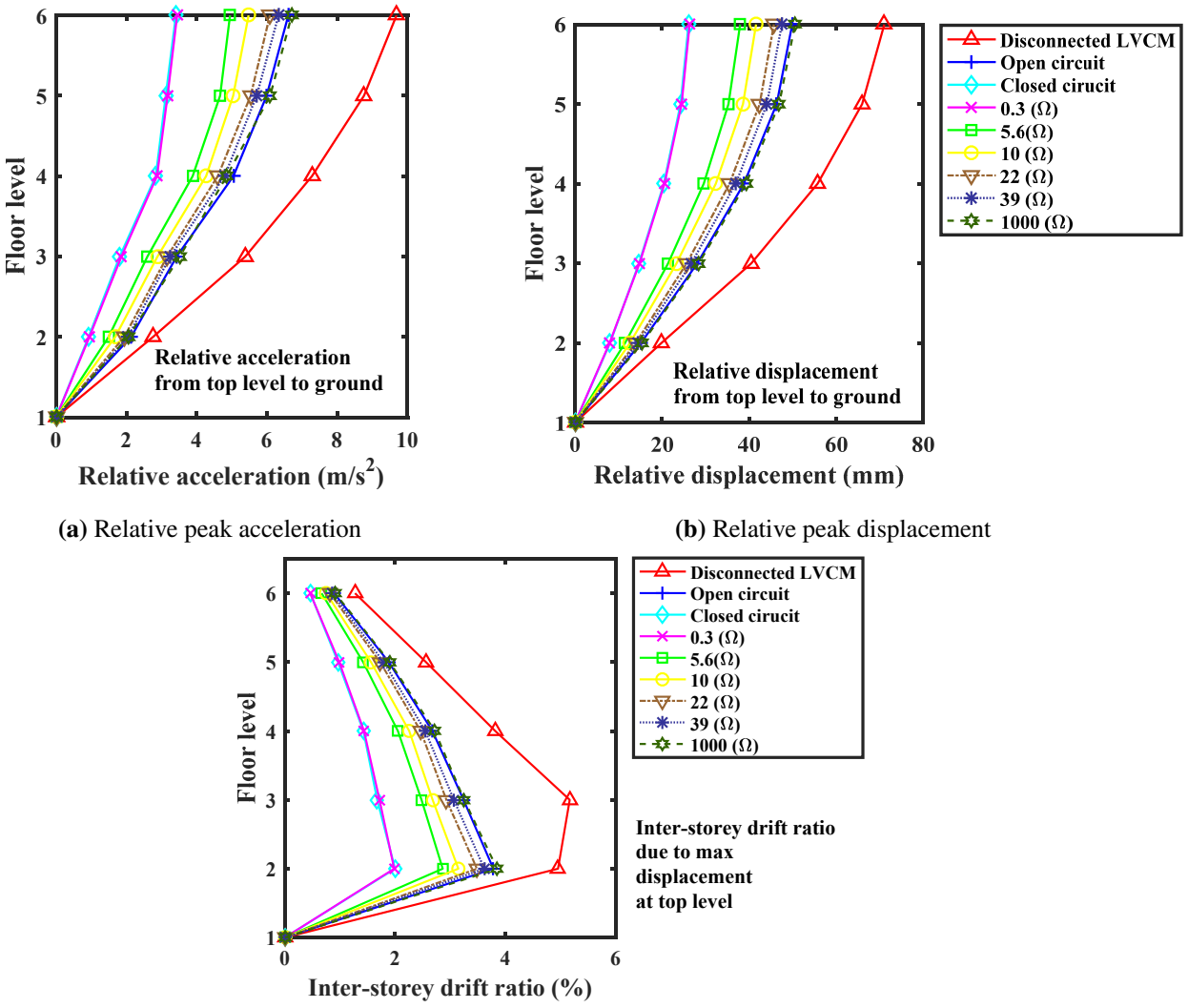

(a) Relative peak acceleration

(b) Relative peak displacement

(c) Inter-storey drift

FIGURE 26 Relative peak acceleration and displacement and inter-storey drift of each level using R shunt circuit (picking the time step of maximum response of the 6F)

the data, the 0.3 Ω resistance case might be approximated as a quasi-linear effect. This could be because of the relatively small displacement between the conductive coil and magnet tube. The 1000 Ω resistance case exhibits obvious nonlinear behaviour, as evidenced by the distorted shapes of the hysteresis loops.

Despite the fact that there appears to be friction in this application, the damping effect of the EMSD using impedance shunt circuits can also achieve a significant reduction in response.

6.2 | EMSD using RLC resonant shunt circuit

Figure 18 b showed the experimental setup of the RLC circuits. It is noted that the RLC resonant shunt circuit is based on two commonly used robust and optimised designs; H_∞ and H_2. Substituting equation 30 into μ_{eq} of equations 16 to 19, the corresponding optimal circuit components are selected in Table 4 .

In the experimental work, the equivalent mass ratio selected (0.08 %) dictates the required magnitude of the capacitor. A non-polarised capacitor, rated at 640 μF, was used for the work. According to the optimal design, the inductor is slightly different for the H_∞ and H_2 designs. In practice, the same value (12000 mH) is used in both cases. The ideal values for the capacitor and inductor are higher than those generally available from electronics suppliers; therefore, they were custom-ordered, with a 10%

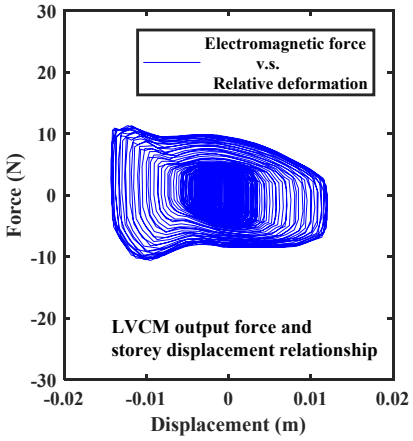

FIGURE 27 Hysteresis relation for shear force and relative displacement under chirp signal input to the AMRF with EMSD using open shunt circuit

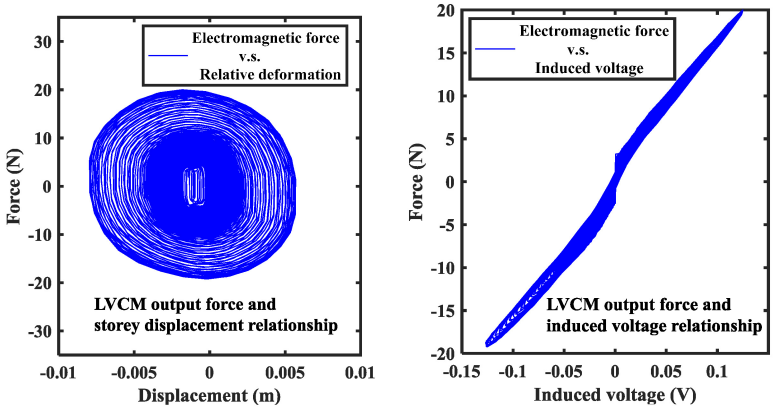

(a) Relation between shear force and relative displacement

(b) Relation between shear force and induced voltage

FIGURE 28 Hysteresis relation for shear force, relative displacement and induced voltage under chirp signal input to the AMRF with EMSD using 0.3 Ω shunt circuit

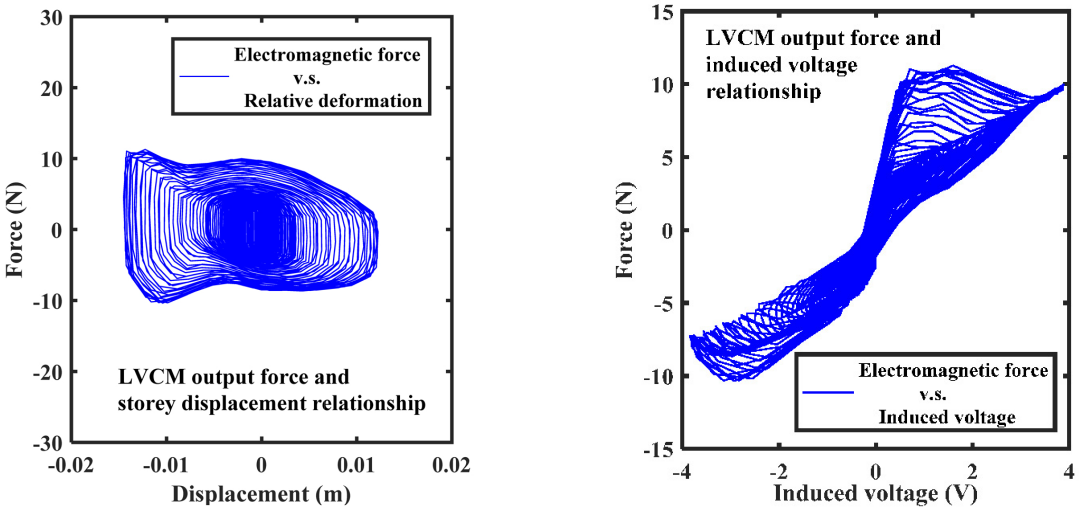

(a) Relation between shear force and relative displacement

(b) Relation between shear force and induced voltage

FIGURE 29 Hysteresis relation for shear force, relative displacement and induced voltage under chirp signal input to the AMRF with EMSD using 1000 Ω shunt circuit

margin of error, directly from the manufacturer. The different optimal designs had different requirements in terms of resistance: H_∞ was 1.83 Ω and H_2 is 0.94 Ω. In practice, resistors of 1.8 Ω and 1 Ω, respectively, were used.

Once the circuit components were set up, a random input was selected to excite the structure. Figures 30 and 31 show the FRF curves for the sixth floor and second floor.

The FRF results show that the H_∞ and H_2 performances do not have the equivalent TMD double-peak feature. The FRF curve seems to have a normal shunt damping effect. This outcome might be due to unexpected friction, nonlinearity between the LVCM and the mounting connection, or alternatively the fabrication of circuit components producing a de-tuning effect in the structural response. Even though the EMSD using RLC does not accomplish the original design expectation, the shunt damping effect does assist in improving the response of the structure.

(Equivalent) mass ratio (%)		0.08	
Single control	Capacitor (μF)	Inductor(mH)	Resistor (Ω)
H_∞	640	12085	1.83
H_2	640	12080	0.94

TABLE 4 EMSD RLC optimal circuit component design using H_∞ and H_2

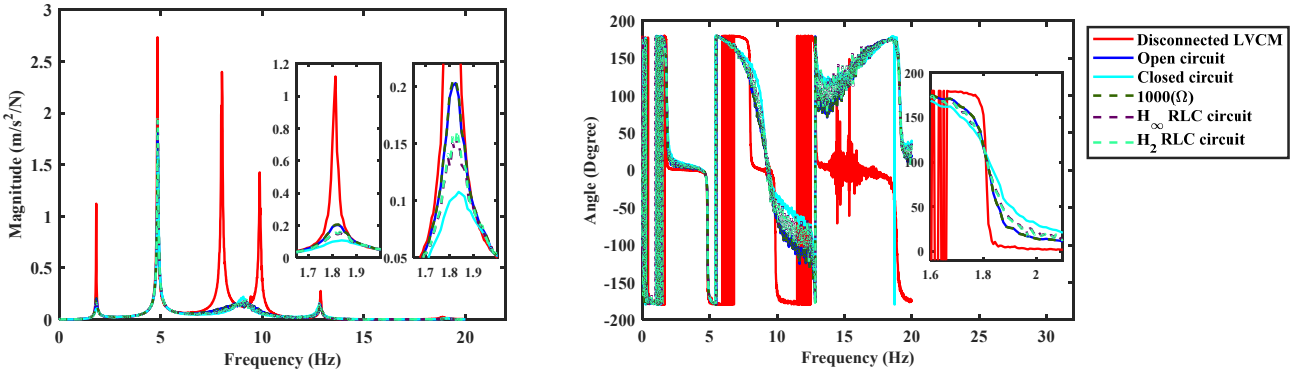

(a) FRF magnitude **(b)** FRF phase

FIGURE 30 6F FRFs of AMRF with EMSD connected and using different RLC shunt circuits

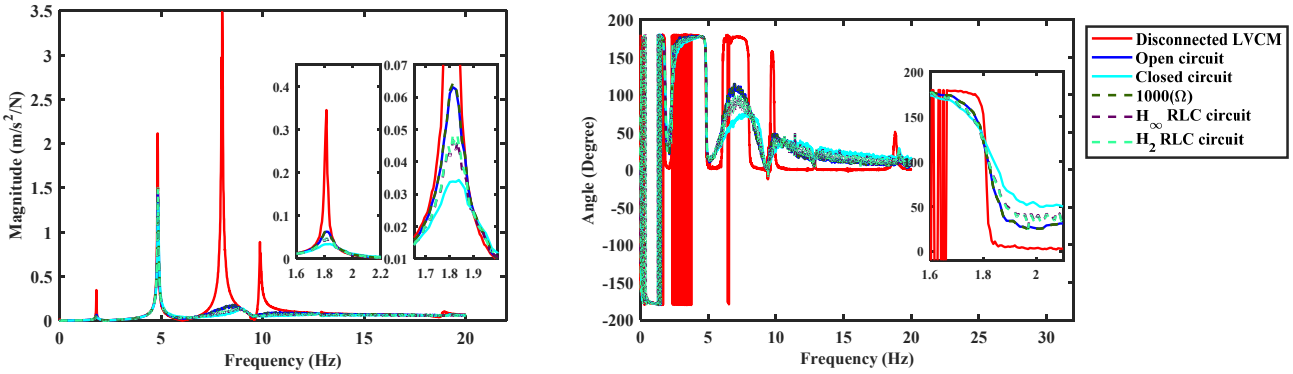

(a) FRF magnitude **(b)** FRF phase

FIGURE 31 2F FRFs of AMRF with EMSD connected and using different RLC shunt circuits

A chirp signal was next applied to the structure to quantify the controlling effect. The frequency range of the chirp signal is from 1.5 Hz to 2.5 Hz to excite the first mode. Figure 32 shows the FRF curves for the sixth and second levels. It can be seen that H_∞ and H_2 show a slight reduction in the first mode frequency.

The EMSD system relies on use of induced voltage. Figure 33 shows the induced voltage time history. If the induced voltage is high, this implies low current and hence damping force, which is the reason on the H_∞ and H_2 RLC shunt circuits produce only a small damping contribution. In this case it is most likely due to detuning of the RLC circuit caused by nonlinear behaviour of the EMSD system.

To further monitor the output force of the EMSD using the RLC shunt circuit, Figure 34 shows the H_∞ and H_2 RLC circuit damper force time histories. The results show that the output force is close to that of the 1000 Ω resistance shunt circuit, which means that H_∞ and H_2 are not providing the optimal response but only providing a small shunt damping contribution.

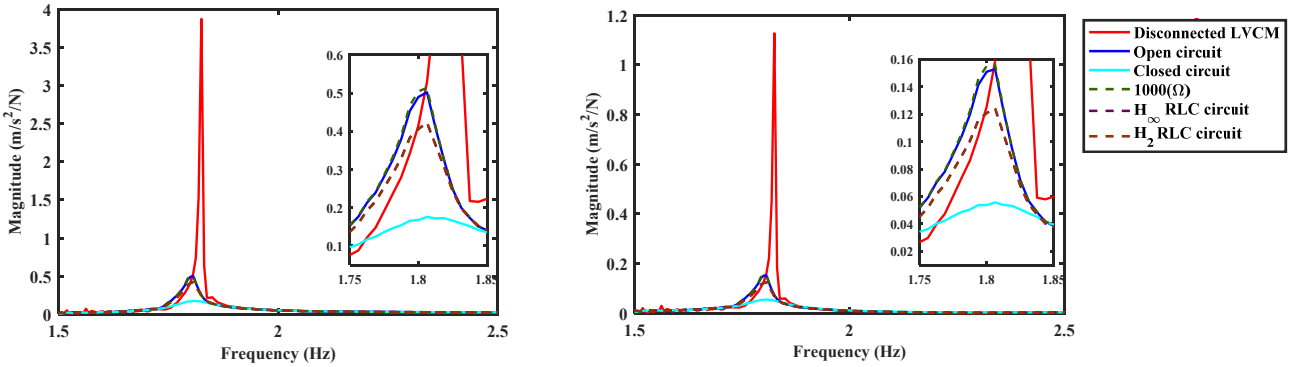

(a) 6F FRF curves **(b)** 2F FRF curves

FIGURE 32 FRFs under chirp signal input to the AMRF with EMSD using different RLC shunt circuits

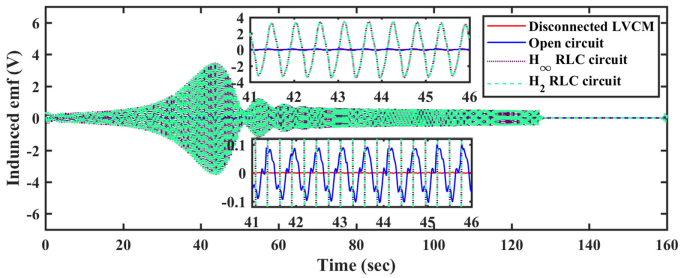

FIGURE 33 Induced voltage time history under chirp signal input to the AMRF with EMSD using different RLC shunt circuits

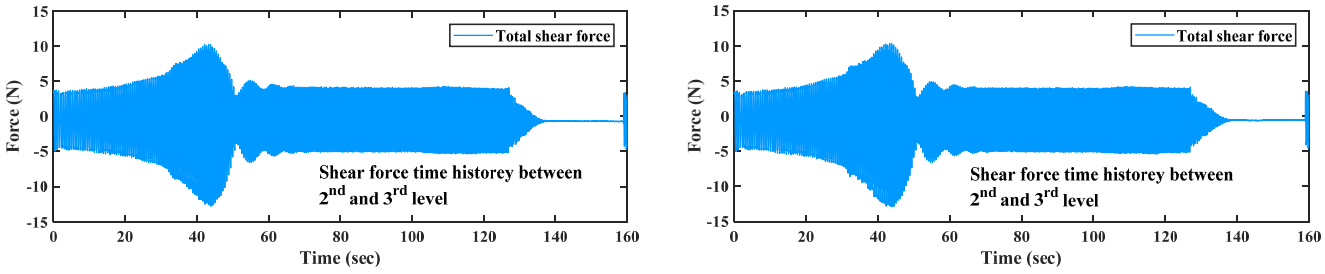

(a) H_∞ RLC shunt circuit **(b)** H_2 RLC shunt circuit

FIGURE 34 Output damping force time history of the EMSD using RLC shunt circuit

Figures 35 a and 35 b show the peak acceleration and displacement. It can be seen that the H_∞ and H_2 RLC circuits produce a slight reduction.

Figure 35 c shows the inter-storey drift. It can be seen that the maximum drift ratio occurs at the second and third level for disconnected LVCM, which is around 4.5-5.0 %. After installing the RLC shunt circuit, this ratio decreases to less than 4 %. Other levels also have different reduction ratios. From this point of view, H_∞ and H_2 also help to improve the structural response; however, the magnitude might not be ideal, as the uncertain nonlinearity creates detuning of the equivalent TMD.

Figures 36 a and 37 a show the hysteresis loops of the damper force and displacement, which exhibit a non-elliptical shape. This may be due to nonlinear effects within the system.

Figures 36 b and 37 b show the damper force and induced voltage relationship; the ideal relation being proportionally linear. However, the results show nonlinear outcomes. The shape of the hysteresis loop and non-proportional relationship suggest the optimal design formula, only fits a linear system and does not fit this non-linear system.

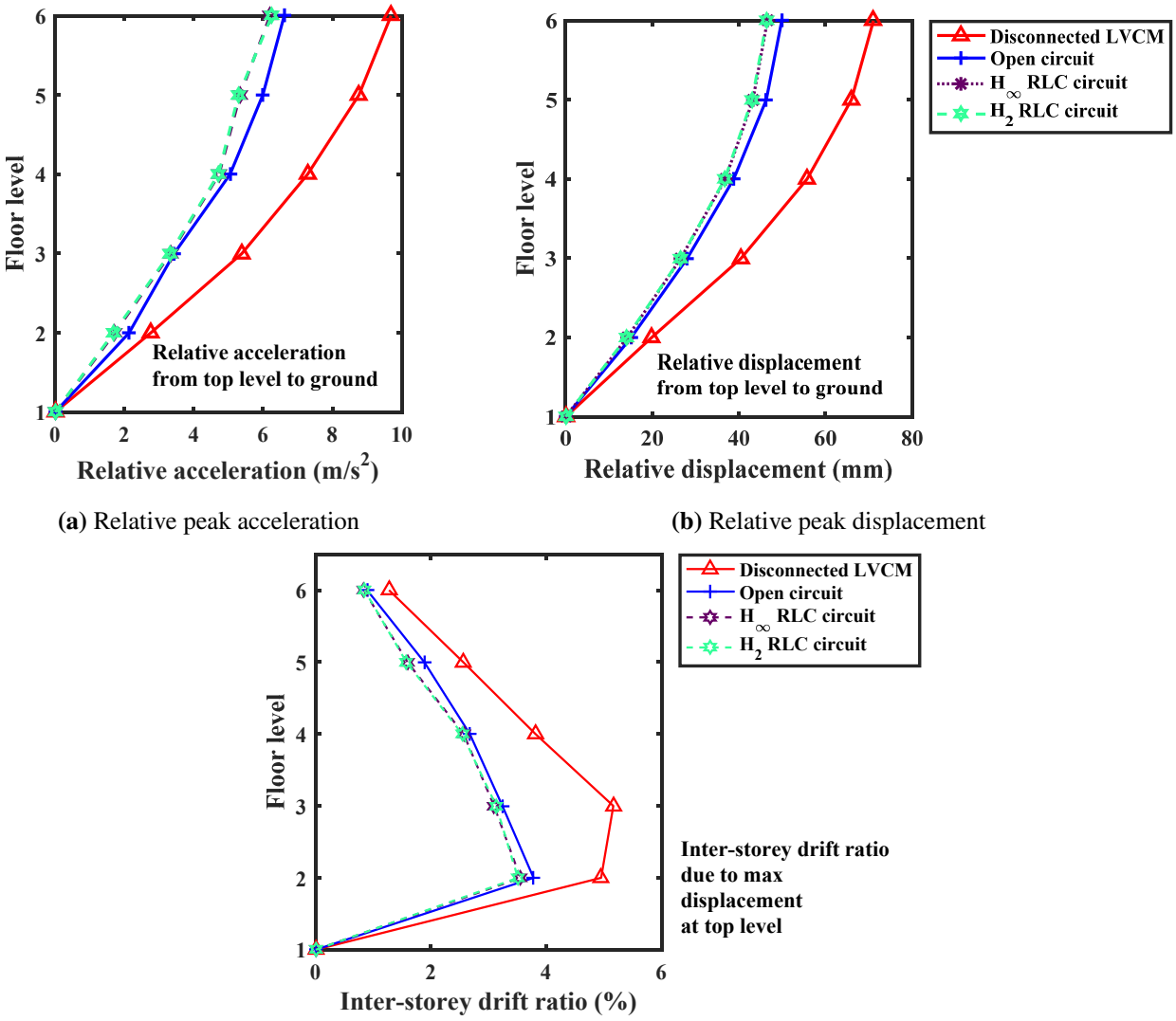

(a) Relative peak acceleration

(b) Relative peak displacement

(c) Inter-Storey drift

FIGURE 35 Relative peak acceleration and displacement and inter-storey drift for each level using RLC shunt circuit

7 | PERFORMANCE EVALUATION

7.1 | VD and EMSD using impedance shunt circuit

In the EMSD application using the impedance shunt circuit, it is conceded that the nonlinearity of the damping system affects its performance. This means that the experimental study result is not the same as that predicted. To understand the influence of the nonlinearity, this subsection compares the FRF curves and evaluates the magnitude of designed damping versus the experimental EMSD shunt damping.

Curve-fitting of the FRF of the AMRF with disconnected LVCM gives a good estimate of the equivalent viscous damping , as evidenced by the regenerated FRF. Figure 38 also shows the FRFs corresponding with the closed circuit, 0.3 Ω and 1000 Ω shunt circuits connected to the EMSD.

Ideally, the designed and measured FRF curves should be almost identical. From Figure 38 it can be seen that the designed and measured FRFs of the lower resistances (closed circuit and 0.3 Ω) have only a slight difference, which is deemed to be acceptable. However, the 1000 Ω case has a large difference. The original design shows no controlling effect, while the measurement of the 1000 Ω case reveals a visible reduction in response; indicating that the 1000 Ω circuit still provides some damping effect. To

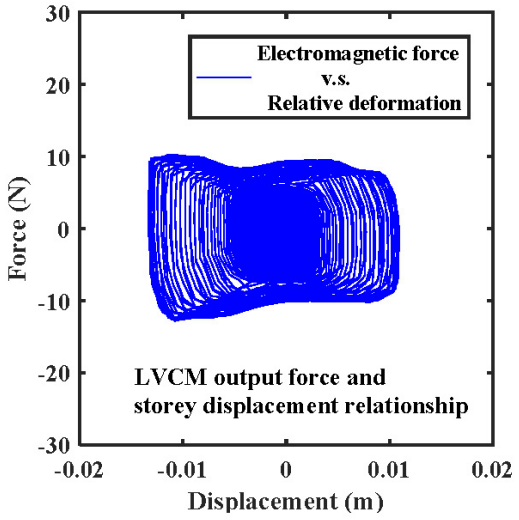

(a) Relation between shear force and relative displacement

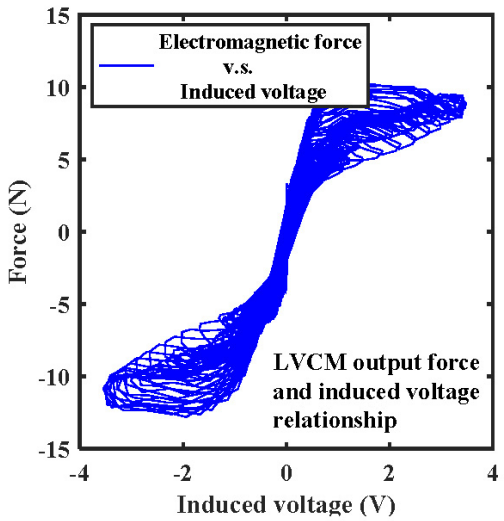

(b) Relation between shear force and induced voltage

FIGURE 36 Hysteretic relationship of shear force, relative displacement and induced voltage under chirp signal input to the AMRF with EMSD using H_∞ RLC shunt circuit

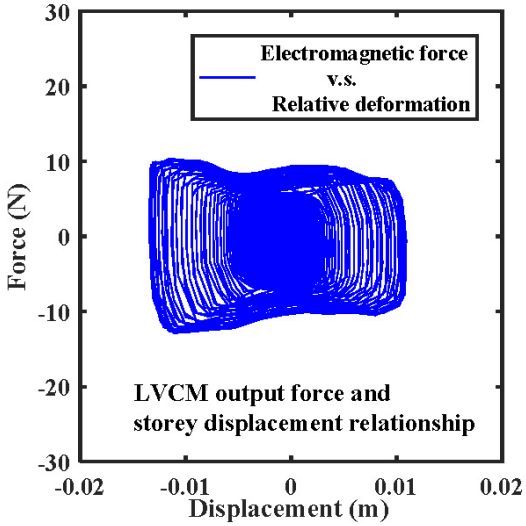

(a) Relation between shear force and relative displacement

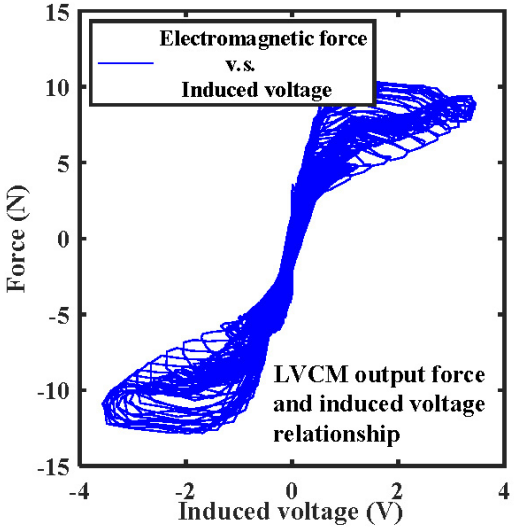

(b) Relation between shear force and induced voltage

FIGURE 37 Hysteretic relationship of shear force, relative displacement and induced voltage under chirp signal input to the AMRF with EMSD using H_2 RLC shunt circuit

quantify the equivalent damping ratio between the designed and measured values, Table 5 illustrates the measured damping ratio for the open, closed and each impedance shunt circuit, based on curve-fitting of the measured FRFs.

In Table 5 it is assumed that the strain energy effective damping of the EMSD (impedance shunt circuits) is the sum of the designed damping and the EMD inherent damping. This is because the measured damping ratio of the EMSD is always higher than that of the original design. The EMSD using impedance shunt circuits adds even more damping to the system. Hence, this result suggests the presence of friction or other source of additional damping.

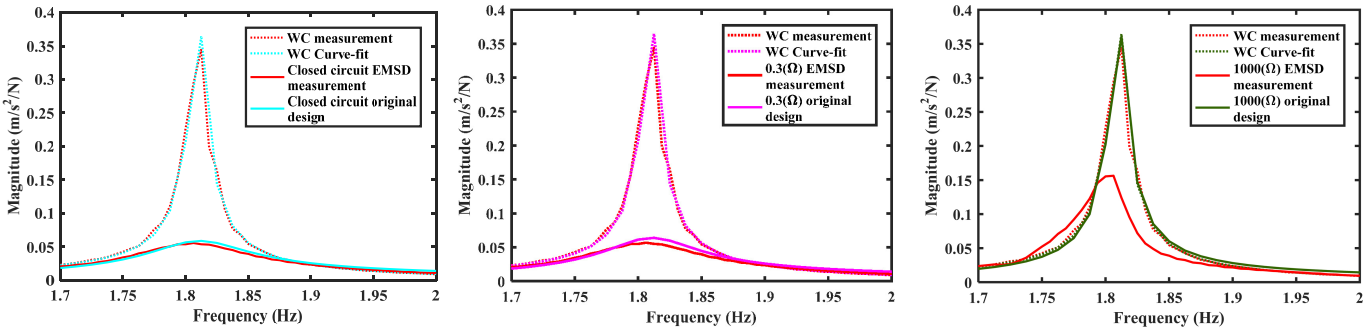

(a) Closed circuit **(b)** 0.3 Ω **(c)** 1000 Ω

FIGURE 38 FRF comparison of the EMSD (impedance shunt circuit) between measured results and simulated design

	Disconnected LVCM	Open circuit	Closed circuit	0.3 Ω	5.6 Ω	10 Ω	22 Ω	39 Ω	1000 Ω
Strain energy effective damping									
Damping ratio of EMSD R shunt circuit (equivalent VD damping) (%)	N/A	N/A	1.49	1.35	0.35	0.34	0.18	0.11	0.00
Model testing curve fitting results									
Overall damping ratio of AMRF with EMSD R shunt circuit(%)	0.33	1.64	3.47	3.37	2.38	2.11	1.91	1.82	1.70
Equivalent damping ratio of EMSD R shunt circuit (%)			1.83	1.73	0.74	0.47	0.27	0.18	0.06

TABLE 5 Comparison of damping ratio between designed damping (equivalent VD damping) and measured damping of the EMSD using impedance shunt circuit

VDs have some potential application problems including viscous liquid leakage issues, and it is not feasible to adjust the magnitude of the damping after installation. However, an EMSD with an impedance shunt circuit might overcome these problems, because the shunt damping relies on the contribution of the circuit components. The magnitude of the EMSD damping can easily be adjusted by changing the value of resistance. The designed value of resistance can be used to match the design requirement conveniently. This concept could avoid replacing the whole damper after discovering functioning non-optimally or if tuning of the damper is desirable, e.g. to achieve optimum damping of a TMD device.

7.2 | TMD and EMSD using RLC resonant shunt circuit

The previous section discussed the performance and evaluation of equivalent viscous damping of an EMD with impedance shunt circuit. However, the predicted performance of the EMSD (RLC circuit) design is similar to that of an equivalent TMD. In this section, the same AMRF structure is used to evaluate the performance of H_∞ and H_2 RLC resonant shunt circuit designs.

The simulated FRFs of the TMD and EMSD using RLC shunt circuits in the frequency domain are shown in Figure 39 . It can be seen that irrespective of H_∞ and H_2 optimal design, they have similar equivalent TMD two lower-peak features.

However, in the experimental application, the H_∞ and H_2 EMSD designs do not have these symbolic features. The result of the EMSD using RLC shunt circuit only provides typical shunt damping. Even though the shunt damping provides greater response reduction, the result reveals that the dynamic performance is not the same as was calculated. This de-tuning effect could be due to a lot of possible reasons. One of the significant issues is the friction which occurs in the fabrication of the LVCM. Moreover, the nominal values of the circuit components have different manufacturer error margins, which might lead to the design of the EMSD failing to perform in an optimal manner, which is worse than the nonlinearity influence.

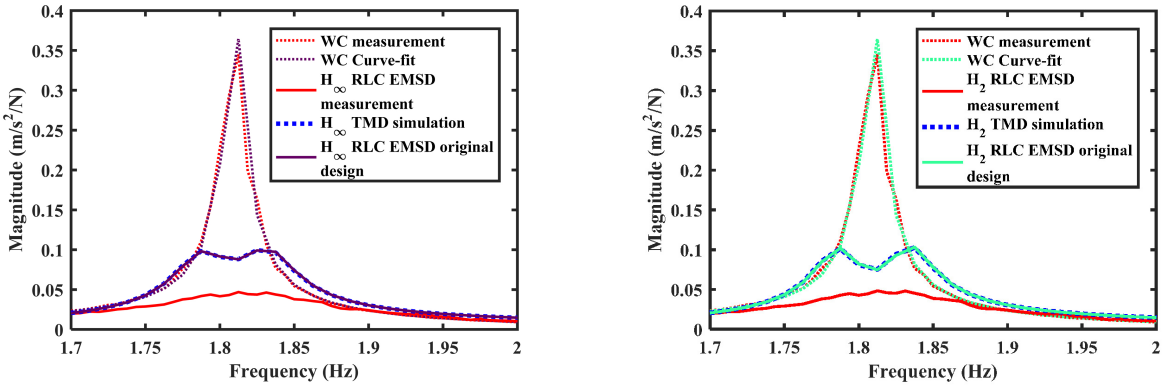

(a) H_∞ RLC circuit **(b)** H_2 RLC circuit

FIGURE 39 FRF comparison of measured results and simulated design results for EMSD using RLC shunt circuit

8 | DISCUSSION AND CONCLUSIONS

In this application, the main objective and new contribution were to investigate the effects of connecting an electromagnetic damper (EMD) with a series of shunt circuits (EMSD). For evaluating the previous findings (novel H_∞ and H_2 robust optimal design formulae) from author study [2, 3], a linear voice coil motor was used as an electromagnetic damping device to extent the study practically. A simple impedance shunt circuit was connected to the EMD with in a laboratory scale frame. The experimental results show that connecting a low value of resistance achieves a better control performance.

The performance of the linear EMSD using an impedance shunt circuit is similar to that of a VD. This type of EMSD design framework was presented through the MDOF strain energy method. The benefit of this shunt damper is the ease with which the damping value can be changed, simply by adjusting the magnitude of the resistor. Modifying the value of impedance to match the control target is more convenient than changing the whole damping system, such as in the case of a VD. This type of EMSD damper does not suffer any liquid leakage problems, and hence has low associated maintenance costs.

When the EMD is connected to an optimally designed RLC oscillating shunt circuit with an MDOF system, the correlated mode decomposition technique was used, and the modified optimal design formulae were proposed to cope with the MDOF system design scheme. Theoretically, the dynamic performance should be the same as that of an equivalent TMD. However, the experimental results did not show the expected performance. The EMSD has a de-tuning effect in comparison with the TMD, which might derive from some nonlinear behaviour of the damper. Even though the controlling results had more reduction, the nonlinearity might be against the damper original design and could not have well response prediction of the damper dynamics.

The identification of this nonlinearity was briefly demonstrated the occurrence of a nonlinearity. However, further experimental studies are needed to verify the possible causes of this.

ACKNOWLEDGEMENT

The authors would like to acknowledge the financial support provided by UK Engineering and Physical Sciences Research Council (EPSRC) through a Leadership Fellowship Grant (Ref. EP/J004081/2) entitled "Advanced Technologies for Mitigation of Human-Induced Vibration".

References

[1] 2019: *Hydraulic Shock Absorbers D-series Linear Dampers*. taylor devices inc.

[2] Ao, W. and P. Reynolds, 2-5 February, 2015: Analysis of h_∞ and h_2 optimal design scheme for an electromagnetic damper with shunt resonant circuit. *Proceedings of IMAC-XXXIII Congress, Orlando, FL, USA*.

[3] Ao, W. K., 2018: *Electromagnetic damping for control of vibrations in civil structures*. The University of Exeter PhD Thesis, Exeter, Devon, United Kingdom.

[4] Ao, W. K. and K. C. Chang, 2010: *Analytical and experimental studies on seismic behavior of structures with building mass dampers*, volume 1. National Taiwan University Master of Science Thesis.

[5] Bae, J.-S., J.-H. Hwang, J.-H. Roh, J.-H. Kim, M.-S. Yi, and J. H. Lim, 2012: Vibration suppression of a cantilever beam using magnetically tuned-mass-damper. *Journal of Sound and Vibration*, **331**, no. 26, 5669–5684.

[6] Behrens, S., A. J. Fleming, and S. O. R. Moheimani, 2005: Passive vibration control via electromagnetic shunt damping. *IEEE/ASME Transactions On Mechatronics*, **10**, no. 1, 118–122.

[7] Behrens, S., A. J. Fleming, and S. Reza Moheimani, 2003: Electromagnetic shunt damping. *Proceedings 2003 IEEE/ASME International Conference on Advanced Intelligent Mechatronics (AIM 2003)*, **2**, no. Aim, 1145–1150.

[8] Cassidy, I. L., J. T. Scruggs, S. Behrens, and H. P. Gavin, 2011: Design and experimental characterization of an electromagnetic transducer for large-scale vibratory energy harvesting applications. *Journal of Intelligent Material Systems and Structures*, **22**, no. 17, 2009–2024.

[9] Chang, K.-C., J.-S. Hwang, and S.-N. Lee, 2004: Status of applications of passive control technologies in Taiwan.

[10] Cheng, T.-H. and I.-K. Oh, 2009: A current-flowing electromagnetic shunt damper for multi-mode vibration control of cantilever beams. *Smart Materials and Structures*, **18**, no. 9, 095036.

[11] Cheng, T.-h. and I.-k. Oh, 2009: Vibration Suppression of Flexible Beam Using Electromagnetic Shunt Damper. *IEEE Transactions on Magnetics*, **45**, no. 6, 2758–2761.

[12] Cheung, Y. and W. Wong, 2011: H2 optimization of a non-traditional dynamic vibration absorber for vibration control of structures under random force excitation. *Journal of Sound and Vibration*, **330**, no. 6, 1039–1044.

[13] Chopra, A., 2007: *Dynamics of Structures: Theory and Applications to Earthquake Engineering*. Prentice Hall International Series in Civil Engineering And, Pearson/Prentice Hall.

[14] Clough, R. and J. Penzien, 1993: *Dynamics of Structures*. Civil Engineering Series, McGraw-Hill.

[15] Den Hartog, J. P., 1985: *Mechanical vibrations*. Dover Publications Inc., New York, 436 pp.

[16] Elliott, S. J. and M. Zilletti, 2014: Scaling of electromagnetic transducers for shunt damping and energy harvesting. *Journal of Sound and Vibration*, 1–11.

[17] FEMA 274, 1997: *NEHRP commentary on the guidelines for the seismic rehabilitation of buildings*. Number October, Federal Emergency Management Agency, 488 pp.

[18] FEMA273, 1997: *NEHRP Guidelines for the Seismic Rehabilitation of Buildings (FEMA Publication 273)*. Number October, Federal Emergency Management Agency.

[19] Fleming, A. J., S. Behrens, and S. O. R. Moheimani, 2003: Active LQR and H2 shunt control of electromagnetic transducers. *42nd IEEE International Conference on Decision and Control (IEEE Cat. No.03CH37475)*, **3**, 2294–2299.

[20] Fleming, A. J. and S. O. R. Moheimani, 2006: Inertial vibration control using a shunted electromagnetic transducer. *IEEE/ASME Transactions On Mechatronics*, **11**, no. 1, 84–92.

[21] Gonzalez-Buelga, A., L. R. Clare, S. A. Neild, S. G. Burrow, and D. J. Inman, 2015: An electromagnetic vibration absorber with harvesting and tuning capabilities. *Structural Control and Health Monitoring*.

[22] Inoue, T., Y. Ishida, and M. Sumi, 2008: Vibration suppression using electromagnetic resonant shunt damper. *Journal of Vibration and Acoustics*, **130**, no. 4, 041003.

[23] McDaid, A. J. and B. R. Mace, 2013: A self-tuning electromagnetic vibration absorber with adaptive shunt electronics. *Smart Materials and Structures*, no. 22, 105013.

[24] Nakamura, Y., A. Fukukita, K. Tamura, I. Yamazaki, T. Matsuoka, K. Hiramoto, and K. Sunakoda, 2013: Seismic response control using electromagnetic inertial mass dampers. *Earthquake Engineering & Structural Dynamics*, 3–4.

[25] Niederberger, D., A. Fleming, S. O. R. Moheimani, and M. Morari, 2004: Adaptive multi-mode resonant piezoelectric shunt damping. *Smart Materials and Structures*, no. 5, 1025–1035.

[26] Niu, H., X. Zhang, S. Xie, and P. Wang, 2009: A new electromagnetic shunt damping treatment and vibration control of beam structures. *Smart Materials and Structures*, **18**, no. 4, 045009.

[27] Palomera-Arias, R., 2005: *Passive electromagnetic damping device for motion control of building structures*. Doctor of philosophy in architecture: Building technology.

[28] Palomera-Arias, R., J. J. Connor, and J. A. Ochsendorf, 2008: Feasibility study of passive electromagnetic damping systems. *Journal of Structural Engineering*, no. January, 164–170.

[29] Scruggs, J. T. and W. D. Iwan, 2003: Control of a civil structure using an electric machine with semiactive capability. *Journal of Structural Engineering*, **129**, no. 7, 951–959.

[30] — 2005: Structural control with regenerative force actuation networks. *Structural Control and Health Monitoring*, **12**, no. 1, 25–45.

[31] — 2006: Optimal nonlocal and asymmetric structural damping using regenerative force actuation networks. *Journal of Engineering Mechanics*, **132**, no. 9, 932–940.

[32] Shen, W., S. Zhu, H. Zhu, and Y.-l. Xu, 2016: Electromagnetic energy harvesting from structural vibrations during earthquakes. *Smart Structures and Systems*, no. August, 2016–2018.

[33] Taylor Device, 1993: San Bernardino county medical center replacement project technical specifications.

[34] Wong, W. O. and Y. L. Cheung, 2008: Optimal design of a damped dynamic vibration absorber for vibration control of structure excited by ground motion. *Engineering Structures*, no. 30, 282–286.

[35] Yan, B., X. Zhang, Y. Luo, Z. Zhang, S. Xie, and Y. Zhang, 2014: Negative impedance shunted electromagnetic absorber for broadband absorbing: experimental investigation. *Smart Materials and Structures*, **23**, no. 12, 125044.

[36] Zhang, X., H. Niu, and B. Yan, 2012: A novel multimode negative inductance negative resistance shunted electromagnetic damping and its application on a cantilever plate. *Journal of Sound and Vibration*, **331**, no. 10, 2257–2271.

[37] Zhu, S., W. Shen, and X. Qian, 2013: Dynamic analogy between an electromagnetic shunt damper and a tuned mass damper. *Smart Materials and Structures*, **22**, no. 11, 115018.

[38] Zuo, L. and W. Cui, 2013: Dual-functional energy-harvesting and vibration control: electromagnetic resonant shunt series tuned mass dampers. *Journal of Vibration and Acoustics*, no. 5.